NACA RM L56J01

NACA

RESEARCH MEMORANDUM

PERFORMANCE OF AN IMPULSE-TYPE SUPERSONIC-COMPRESSOR ROTOR HAVING A MEAN TURNING OF 114°

By Theodore J. Goldberg and John R. Erwin

Langley Aeronautical Laboratory
Langley Field, Va.

NATIONAL ADVISORY COMMITTEE
FOR AERONAUTICS

WASHINGTON

January 7, 1957
Declassified October 31, 1958

NATIONAL ADVISORY COMMITTEE FOR AERONAUTICS

RESEARCH MEMORANDUM

PERFORMANCE OF AN IMPULSE-TYPE SUPERSONIC-COMPRESSOR ROTOR HAVING A MEAN TURNING OF 114°

By Theodore J. Goldberg and John R. Erwin

SUMMARY

A 16-inch tip-diameter rotor designed for impulse operation at the mean radius with a relative Mach number of 1.53 and 114° of turning was designed to produce an isentropic pressure ratio of 13 to 1 and a weight flow of 28 pounds per second at a tip speed of 1,370 feet per second in air. The rotor was designed to permit the mean particle path to flow through the rotor in a plane rather than the usual spiral path about the axis of rotation in order to alleviate the very large downstream radial static-pressure gradient which would otherwise result from the high turning in the rotor.

Although the rotor was designed to operate in air, all tests were made in Freon-12. Performance of the rotor alone, rotor with guide vanes, and the rotor-guide-vane configuration with sheet-metal stators was obtained over a speed range of 58 percent to 119 percent of design speed.

At design speed, the rotor operating with guide vanes produced a total-pressure ratio of 9.6 and an efficiency of 85.5 percent with a weight flow of 46.7 pounds per second of Freon-12. Without guide vanes, the values were 9.2, 89.2, and 44.4, respectively. The average absolute discharge Mach number was about 2.1 at an average angle of about 65°.

At all speeds tested, a region of separated recirculating flow was observed at the hub downstream of the rotor as a result of the inward centrifugation of the boundary layer in conjunction with a rising pressure gradient along the hub contour. The presence of sheet-metal stators behind the rotor eliminated this recirculating flow and produced a more nearly uniform exit flow, although the overall performance remained essentially the same as that obtained without the stators.

INTRODUCTION

An analytical study of supersonic axial-flow compressors made in reference 1 has indicated that, for a single stage having subsonic velocity into the stator, the limiting total-pressure ratio is about 3.5. Several compressors of this type, which were experimentally investigated and reported in references 2 to 4, have demonstrated a serious problem in subsonic diffusion because of shock-boundary-layer interaction. By permitting supersonic velocities at the stator entrance, a compressor having supersonic flow throughout the rotor may be utilized to obtain higher total-pressure ratios. The problem of shock-boundary-layer interaction together with efficient diffusion is placed on the stator where more elaborate techniques may be employed.

An impulse-type supersonic compressor has no, or very little, static-pressure rise through the rotor and the energy input to the gas is achieved by large turning of the flow at supersonic velocities. The flow leaving the rotor is supersonic and must be diffused in the stators to subsonic velocity where the kinetic energy imparted by the rotor is converted to static pressure. It has been shown in reference 5 that large turnings can be efficiently accomplished, and in reference 6 results of cascade investigations of supersonic turning passages are used to estimate the performance characteristics of this type of supersonic compressor.

Because of the promising cascade results, it was decided to investigate a high-turning rotor of the impulse type to explore the capabilities and problems associated with high-pressure-ratio single-stage compressors. A high-solidity rotor having an inlet hub-tip radius ratio of 0.75 with a 16-inch tip diameter and an exit hub-tip radius ratio of 0.795 with a 16.6-inch tip diameter was designed to produce an isentropic pressure ratio of about 13 to 1 at a tip speed of 1,370 feet per second in air with a weight flow of 28 pounds per second in air. The blading was designed for impulse-type operation at the pitch with a relative inlet Mach number of 1.53 and 114° of turning in the rotor passage. The high discharge tangential velocity produced by the rotor would produce an extremely large static-pressure gradient downstream of the rotor if a conventional flow path were employed. In this compressor, the particles were permitted to flow through the rotor in a plane rather than in the usual spiral path about the axis of rotation, as will be explained subsequently. Although the rotor was designed aerodynamically and structurally to operate in air, all tests were made in Freon-12 which permitted testing at about one-half the rotational speed required in air and alleviated a high-bearing-temperature problem. Rotor performance with and without the design guide vanes was obtained

through a speed range of 58 percent to 119 percent of design speed. In addition, preliminary tests with sheet-metal stators were conducted.

SYMBOLS

a	velocity of sound, ft/sec
c_p	specific heat at constant pressure, $ft^2/sec^2/^oR$
g	acceleration due to gravity (32.2 ft/sec^2)
M	Mach number, ratio of flow velocity to velocity of sound, V/a
n	rotational speed of rotor, rps
P	total or stagnation pressure, lb/ft^2
p	static pressure, lb/ft^2
Q	torque, ft-lb
r	radial position measured from axis of rotation, ft
T	total or stagnation temperature, ^oR
t	static temperature, ^oR
ΔT	measured stagnation-temperature rise, ^oR
$\Delta T'$	isentropic stagnation-temperature rise, ^oR
U	rotational velocity of blade element, $2\pi rn$, ft/sec
V	velocity of fluid, ft/sec
W	weight flow, lb/sec
β	angle between axial direction and flow direction, deg
γ	ratio of specific heats
δ	ratio of actual inlet total pressure to standard sea-level pressure, $\frac{P_i}{2116}$

η_m momentum efficiency, $\frac{C_p \Delta T'}{U_2 V_{u,2} - U_1 V_{u,1}}$

η_Q torque efficiency, $\frac{C_p \Delta T' W}{2\pi n Q g}$

η_t temperature (adiabatic) efficiency, $\frac{\Delta T'}{\Delta T}$

θ ratio of actual inlet stagnation temperature to standard sea-level temperature, $\frac{T_i}{518.6}$

ρ density, slugs/ft^3

ϕ turning angle, rotor coordinates, deg

$W \frac{\sqrt{\theta}}{\delta}$ equivalent weight flow, lb/sec

$U_t/\sqrt{\theta}$ equivalent tip speed, ft/sec

Subscripts:

a axial component

h hub

i settling chamber

t tip

u tangential component

1 rotor entrance, stationary coordinates

1R rotor entrance, rotor coordinates

2 rotor exit, stationary coordinates

2R rotor exit, rotor coordinates

COMPRESSOR AERODYNAMIC DESIGN

GENERAL CONSIDERATIONS

At the time this compressor was designed, several shock-in-rotor supersonic compressors had been constructed and tested (refs. 2 to 4). These reaction compressors had failed to produce the pressure ratios predicted for them. The differences were largely due to the inability to attain the necessary large static-pressure rise because of flow separation and poor diffusion in the rotor resulting from shock-boundary-layer interaction. The impulse rotor was intended to overcome this difficulty by adding only kinetic energy to the flow and requiring little or no static-pressure rise through the rotor. Since impulse turbines operate with acceptable efficiencies, there was reason to believe that an impulse compressor could be made to work efficiently if the static-pressure rise was transferred entirely to the stator. Boundary-layer control, high solidities, movable and multiple blade rows could be applied to stator blades to cope with the difficult diffusion problem.

In the design of the rotor, it was desired that the turning angle produced by the rotor be twice the relative air inlet angle. This permits "impulse" conditions to exist without a large contraction of the annulus area. However, this high turning produces a serious problem in the design of an impulse compressor rotor. The problem results from a very large radial static-pressure gradient due to the high tangential velocity of the flow downstream of the rotor. In order to alleviate this problem, the rotor was designed so that a particle is permitted to flow through the rotor in a plane rather than in the usual spiral path about the axis of rotation. These considerations provide a close approach to a two-dimensional flow in the rotor and simplify the rotor design by allowing the direct use of two-dimensional blade section.

ROTOR DESIGN

Inlet Conditions

The inflow velocity distribution was selected as follows:

(1) A hub-tip radius ratio of 0.75 and a tip diameter of 16 inches

(2) A rotational speed of 1,200 feet per second at the mean radius

(3) An inlet axial Mach number of 0.80 at the tip diameter

This value reduces the mass flow only about 3.7 percent below the maximum that would occur with sonic velocity, but permits the use of guide vanes without local supersonic velocities.

(4) 0° guide-vane turning at the tip section

(5) Constant total pressure relative to the rotor at all radii

This condition was chosen to minimize the secondary flow and mixing losses within the rotor.

Exit Conditions

Initial calculations to determine the exit flow conditions were made with the assumption of impulse operation at the mean radial station and a turning angle at each radial station equal to twice the relative inlet angle. Assuming a constant radius through the rotor at all radial stations and satisfying simple radial equilibrium as well as continuity resulted in a hub-to-tip static-pressure variation from about $0.07p_1$ to $2.06p_1$ and an absolute Mach number variation from about 5.0 to 1.9. It can be seen that a significant variation from two-dimensional flow would result if provisions were not made to alleviate these conditions.

Since simple radial equilibrium for flow through concentric cylinders parallel to the axis could not be satisfied without producing a large static-pressure gradient, a solution to the problem was attempted by arbitrarily selecting a small static-pressure variation from the mean radius and satisfying radial equilibrium by contouring the hub and tip so that a particle in the mean streamline between blades would flow through the rotor in a plane rather than in a spiral path about the axis of rotation (see fig. 1(a)). In order to determine the rotor hub and casing contours that would accomplish this purpose, detailed plots were made from two-dimensional blade layouts of the mean streamline particle paths in stationary coordinates at each of the three radial stations. The displacement curve of the particle path for the tip section is shown in figure 1(b). The streamline path in the meridional plane (a plane containing the axis of rotation) which would permit each particle to remain in a single plane was then determined for three radial stations. As was to be expected, little curvature in the meridional plane was required until the last 20 to 30 percent of the chord is reached. It was found that minimum curvature of the rotor hub and outer casing contours would result if the entrance flow were inclined at an angle to the axis of rotation. For reasons of practical construction and running clearance, it was decided to compromise the ideal contours and use conical surfaces of 10° for the rotor hub and 6° for

the outer casing. The difference between the conical surface and the required casing shape determined from the particle path of the mean streamline can be seen in figure 1(c). Although the required slope of the casings increases sharply near the trailing edge of the rotor, as seen in figure 1(c), the selected conical surfaces were continued downstream of the rotor. It was realized that this would not allow each particle to continue in the same plane downstream of the rotor; therefore, the flow within the rotor would be affected. In order to alleviate this condition, the stator blades were to be placed very close to the rotor to reduce the tangential velocity as quickly as possible. Because the use of stators was intended, no special contouring of the stator casing was attempted.

BLADE SECTION DESIGN

The concepts employed in designing the blade sections for this rotor were as follows: It was desired to turn the flow through the required angle with a minimum static-pressure rise on the blade surface. This was particularly true of the convex surface, since the static-pressure rise must occur near the trailing edge in the presence of a developed boundary layer. The optimum pressure distribution was believed to exhibit nearly constant pressures on both convex and concave surfaces. It was then believed best to avoid decelerating through a Mach number of 1, because doing so was expected to produce strong normal shocks and separation. Rather arbitrary limits of surface Mach number were selected with Mach numbers of 1.25 and 2.50 chosen as constant values for the concave and convex surfaces, respectively.

The blade sections were designed by using the method of characteristics for two-dimensional flow for the three radial stations, hub, mean, and tip, based upon inlet radii. From these layouts, the mean stream-line particle paths were computed to determine the casing slopes. In order to adjust for annular-area change due to the converging slopes of the casings, the turning angles were reduced by an amount necessary to satisfy continuity and the required static pressures. In addition, an area increase of 10 percent was allowed for boundary-layer blockage. At the time these blade sections were designed, in 1948, the application of supersonic vortex flow to supersonic turning passages (ref. 7) had not been realized. Since a systematic method of blade-section design was not then available, a number of trials were made to obtain sections which were acceptable by themselves and compatible with each other in a three-dimensional blade form. The resulting layout for the tip section showing the characteristic network is presented in figure 2.

The final aerodynamic design for this rotor was a result of a trial-and-error process to determine the casing slopes and turning angles which

satisfied the assumed static pressures at the rotor exit. The final flow parameters are tabulated in figure 3(a) for air. The resultant mean values of isentropic total-pressure ratio and weight flow are 13 and 28 pounds per second of air, respectively. Because all tests were made in Freon-12, the original air design has been converted to corresponding values for Freon-12 by the method described in reference 4. The flow parameters for Freon-12 are tabulated in figure 3(b).

In order to permit starting and efficient diffusion of the flow at the high rotor discharge Mach numbers on the order of 2.6, it was felt that movable stators would be necessary. However, before the stator design was attempted, it was decided first to obtain experimentally the rotor discharge flow conditions.

APPARATUS AND METHODS

TEST STAND

The impulse-type supersonic compressor was tested with Freon-12 as a working fluid in a closed system described in reference 8. A sectional view of the installation is presented in figure 4 and the details of the annulus in the region of the rotor are shown in figure 5. The compressor rotor was driven through a 2:1 gear-ratio speed increaser by a 3,000-hp variable-frequency induction motor. The motor drive shaft was adapted for a wire strain-gage-type torquemeter.

TEST COMPRESSOR

The rotor was designed to have 50 blades and a rotor hub width of $2\frac{3}{4}$ inches. The blade sections, designed graphically by the method of characteristics for two-dimensional flow, have a constant chord of 2.73 inches. The ordinates of the three sections, hub, mean, and tip, are presented in table I. The rotor disk was machined from 2014-T6 aluminum-alloy forging and the rotor blades from 7075-T6 aluminum-alloy bar stock. The blades were held in the rotor by a fir-tree method of attachment and were held in place by screws in threads tapped half in the rotor and half in each blade. A photograph of the test rotor appears in figure 6.

The guide vanes, which were machined from duralumin, were located upstream of the rotor between an annulus of constant inner and outer radii. The annulus area was 10.7 percent greater than that at the

rotor entrance to reduce the possibility of choking the flow at the vanes. Twenty-one guide vanes, having a constant chord of 2.45 inches, were used. The guide vanes were designed by use of the data of reference 9. Details of the guide-vane sections are presented in figure 7.

In an attempt to eliminate the influence of the downstream static pressure on the rotor, a set of sheet-metal stators was installed $1\frac{3}{16}$ inches behind the rotor. The stators were fabricated from $\frac{1}{16}$-inch steel plate bent to a circular-arc shape generated by a $10\frac{3}{4}$-inch radius. The blades had a 15° leading-edge wedge angle and were so oriented that the flow at the design angle entered tangent to the suction surface at the leading edge. Twenty-one blades having a constant chord length of 4.8 inches resulted in a solidity of 2.1 at the mean radius.

INSTRUMENTATION

Measurements at the inlet to the compressor were made in the settling chamber, as recommended in reference 10. Four static-pressure orifices spaced 90° apart were used to measure the total pressure, and four thermocouples located at the area centers of equal annular areas were used to determine the stagnation temperature.

The inner and outer walls upstream and downstream of the rotor as well as the casing over the rotor were extensively instrumented with static-pressure orifices. Eight static-pressure taps, spaced 45° apart, were provided on both the inner and outer walls at the measuring stations located 1 inch ahead of and 3/4 inch behind the rotor.

A combination pitot-static-yaw survey probe and a single-bell, shielded thermocouple probe similar to those shown in reference 8 were used at the downstream measuring station; a claw-type yaw instrument was used to measure the rotor inlet angles. The probe heads were alined for the mean casing angle of 8°. All survey probes were mounted in a remotely operated, motor-driven survey mechanism which provided separate control for rotation and traverse.

The weight flow through the compressor was measured by a calibrated venturi located as shown in figure 4.

All pressures were recorded simultaneously by photographing multiple-tube mercury manometer boards. Commercial self-balancing potentiometers indicated the temperatures taken with calibrated iron-constantan thermocouples and the work input, or power absorbed by the rotor, as measured by a wire strain-gage-type torquemeter. Automatic control valves were used to maintain constant preset values of settling-chamber pressure and temperature during test runs by controlling the

rate of flow of cooling water and Freon-12. The rotor speed was measured by a commercial stroboscopic tuning-fork-controlled instrument.

The velocity of sound in the Freon-air mixture was measured by an instrument similar to that described in reference 11. From this measurement, the proportions of the gas constituents and the physical characteristics of the mixture were determined.

PROCEDURE

The performance of the rotor with and without guide vanes and with sheet-metal stators was obtained in Freon-12 over an equivalent tip-speed range of 58 percent to 119 percent of design speed. The inlet stagnation pressure varied from 0.50 atmosphere for low-speed runs to 0.10 atmosphere for high-speed runs with a corresponding variation in test gas purity from about 99 to 90 percent by volume of Freon-12. The values for the gas properties corresponding to the purity measured for each test were used in the performance calculations.

Flow conditions entering the rotor were determined from the stagnation pressure and temperature in the settling chamber and an assumed straight-line variation between the averages of the inner- and outer-wall static taps 1 inch ahead of the rotor. Flow angles leaving the guide vanes were determined by using an external air supply ducted into the test stand and, with the rotor removed, surveying radially at the axial station at which the rotor leading edge would be located.

Since the exit Mach numbers are highly supersonic, on the order of 2.5, the true total pressure must be obtained from normal shock relationships and measured pitot and static pressures. In this range of Mach number, the pitot correction is a highly sensitive function of static pressure and, therefore, the accurate measurement of the static pressure is essential.

For the initial test runs, total-pressure and total-temperature rakes as well as a pitot-static-yaw probe were installed at the downstream measuring station. However, these results were discarded because of large interference of the instruments on the wall static pressures as well as mutual interference between the instruments. Successive tests were made with different instruments at various circumferential locations but the large interference effects could not be eliminated. The interference pattern of circumferential inner- and outer-wall static-pressure measurements varied with survey position of each probe as well as with rotor speed. With the probes against the outer casing, the

variation in circumferential static pressure was as high as 20 percent of the minimum reading for both the outer- and inner-wall taps. In addition, different types of combination pressure-yaw probes located at the same circumferential position produced a difference in radial variation of static pressure of as much as 50 percent of the minimum readings which resulted in a 40-percent difference in total-pressure ratio across the rotor. The mutual interference of the instruments can be attributed to the existence of a subsonic axial discharge Mach number.

The downstream instrumentation was finally reduced to one combination pitot-static—yaw probe, carefully calibrated for static pressure for Mach numbers up to 3.0, and one single-bell, shielded temperature probe. A radial survey was made first with the pitot-static—yaw probe while the temperature probe was kept against the outer wall, and then a temperature survey was made with the combination pressure-yaw probe against the outer casing. This eliminated the interference between the survey probes, but considerable effects on the wall static measurements were still noted. The radial static-pressure distribution was obtained by fairing through the pressure measurements of the survey probe to the average of the readings of the wall static taps which showed no, or very little, variation with survey-probe position.

The radial distributions of all measured parameters were faired as a family for each configuration; that is, all tests with guide vanes at open throttle, all tests with guide vanes at maximum back pressure, and so forth. This method produced results which are felt to be valid because the work input measured by momentum change and temperature rise agreed with the work input determined from torque measurements.

REDUCTION OF DATA

The derived quantities at each radial station were computed from the measured data as described in the appendix of reference 3 except for the inlet Mach numbers, which were based upon an assumed straight-line variation between the inner- and outer-wall static pressures. The values of γ and velocity of sound used in these calculations were obtained from the equations given in reference 11. For computations of parameters at each measuring station, the value of γ was based upon an average of the static and total temperatures, but, for obtaining parameters across the rotor, the value of γ was based upon an average of inlet and exit total temperatures. For the blade-element calculations, the streamlines were assumed to be the loci of radii of equivalent percentage passage height at each station.

The overall total-pressure ratios were computed by using the inlet stagnation conditions measured in the settling chamber and a mass-weighted average of the downstream total pressures which were corrected for normal shock losses.

In addition to the weight flow obtained from a calibrated venturi, the weight flow upstream and downstream of the rotor was obtained by integration of the elemental weight flow at each radial station. The values of the inlet weight flow were within 2 percent of those obtained by the venturi; the values of the exit weight flow were up to 7 percent higher than those measured with the venturi. All values of weight flow presented are those measured by the venturi.

Three methods were used to determine the rotor efficiency: the first, designated η_t is based upon measured total-temperature rise; the second, η_M is based upon momentum change across the rotor, and the third, η_Q is based upon torque measurements to obtain the actual power absorbed. Efficiencies computed by the three methods are presented except for those test runs during which the torque measuring device failed.

During tests of the rotor without stators, the exit-flow directions indicated a region of reverse flow near the hub. Since this reverse flow is indicative of a circulatory flow which is not capable of producing any useful work but, nevertheless, must absorb some portion of the work input to the rotor, it was necessary to reexamine the procedure to determine mass-weighted values of total-pressure ratio and efficiency as presented in the appendix of reference 2. Typical curves showing the radial distribution of exit mass flow and temperature rise are presented in figure 8. The radius of the limiting stream line which divides the through flow from the circulatory flow was obtained for each test run by integration so that positive area B is equal to the negative area A for the curve of $\rho_2 V_{a,2}$. All output parameters such as $\left(P_2/P_1\right)\rho_2 V_{a,2}$ and $C_p \Delta T' \rho_2 V_{a,2}$ were integrated from the tip r_t to this limiting streamline r_b where as the input parameters such as $C_p \Delta T \rho_2 V_{a,2}$ and $U_2 V_{u,2} \rho_2 V_{a,2}$ were integrated from r_t to r_h. In this way, the work necessary to maintain the circulatory flow is charged to the rotor.

RESULTS AND DISCUSSION

Aerodynamic performance data of the experimental compressor were taken in Freon-12 for the rotor with and without guide vanes and for the rotor—guide-vane combination in the presence of sheet-metal stators.

In addition, tests were run with the rotor alone after modifying the hub contour.

ROTOR WITH GUIDE VANES

Overall Performance

The overall performance of the rotor operating with guide vanes is presented in figure 9 in terms of total-pressure ratio, efficiency, and equivalent weight flow as functions of equivalent tip speed. The weight flow and compressor tip speed have been converted to equivalent values for air by the methods described in the appendix of reference 4.

Open throttle.- For the open-throttle condition, a maximum efficiency of 94.5 percent was obtained at an equivalent tip speed of 366 feet per second with a total-pressure ratio of 3.1 and a weight flow of 36.7 pounds per second of Freon-12. The efficiency decreased with increasing rotor speed to 85.5 percent at the design speed of 626 feet per second (equivalent value for air, 1,370 feet per second) where the total-pressure ratio was 9.6 and the equivalent weight flow was 46.7 pounds per second of Freon-12 (air equivalent value, 24.9 pounds per second). Thereafter, the efficiency remained constant at 85.5 percent to the maximum speed tested, 119 percent of design, where a total-pressure ratio of 18 and a weight flow of 48.7 pounds per second of Freon-12 were measured.

The value of total-pressure ratio measured at design speed does not agree with the design values. However, it should be remembered that the estimated Freon-12 values presented in figure 3 are based upon 100-percent efficiency. At these high pressure ratios, a small change in efficiency produces a large change in pressure ratio. For example, the isentropic value of 16.7 would drop to 11.5 at an efficiency of 85 percent for the same work input. In addition, if impulse operation is to be maintained at the mean section, a reduction in efficiency results in a lower exit velocity. Therefore, the work input would be reduced which would further decrease the pressure ratio.

Effect of back pressure.- Increasing the back pressure, by closing the throttle, had no effect on the weight flow over the entire speed range tested (fig. 9). Previous impulse-type supersonic compressors, reported in references 12 to 14, exhibited a range of weight flow with throttling, small at design speed but increasing with decreasing tip speed. It is not known whether this difference is due to the higher turning of the rotor in the present investigation (114° compared with about 60° for refs. 12 to 14) or whether it is due to test-rig effects.

Over most of the throttling range the total-pressure ratio and efficiency remained constant. However, at maximum throttle, the point just before audible surge, the total-pressure ratio and efficiency were reduced by about 20 percent and 6 percent, respectively. A decrease in total-pressure ratio with increased back pressure is a characteristic of rotors turning past axial. This can be readily seen from a typical velocity diagram. Inasmuch as some diffusion is obtained in the rotor from increased back pressure, the relative exit velocity is reduced; if the turning in the rotor is assumed to remain the same, the vector addition of the rotational speed results in a decrease in the tangential component of the absolute exit velocity, and thus a decrease in work input.

The effect of back pressure on the static pressure distribution along the outer casing is shown in figure 10. At 98 percent of design speed (fig. 10(a)) the profile is typical of the distribution obtained at all speeds above 59 percent of design speed (fig. 10(b)) although the absolute values varied with rotor speed. At 98 percent of design speed increasing the back pressure had no effect on the pressures along the casing until the maximum throttle point was reached. This indicates that no diffusion could be obtained in the rotor until the point just before surge and substantiates the constant total-pressure ratio obtained at the downstream measuring station over most of the throttling range. At the point of maximum back pressure, only the casing pressures downstream of the rotor leading edge were affected. The pressures upstream of the rotor remained independent of throttling indicating that a shock could not be stabilized ahead of the rotor, and, therefore, the weight flow could not be affected.

Blade-Element Performance

The variation of several parameters at several tip speeds for the open and maximum throttle conditions are presented in figures 11 to 16 as functions of radial position. Since the intermediate throttle conditions had no effect on the rotor performance as seen in figure 10(a), only the open and maximum throttle conditions are discussed throughout the paper.

Inlet conditions.- The absolute inlet flow angles, shown in figure 11(a), are in good agreement with the design values at the tip and root but are about 3.5° higher than predicted at the pitch section. The relative inlet flow angles, also shown in figure 11(a), were greater than the design inlet angle at all speeds. Therefore, the rotor operated at a positive angle of attack, herein defined as the angle between the relative upstream undisturbed flow direction and the straight portion of the suction surface just behind the leading-edge radius. The increase in angle of attack with increasing tip speed is attributed to

the blunt leading edge and is in agreement with the two-dimensional analysis for curved entrance regions, or cambered blades of reference 15.

The relative inlet Mach number, presented in figure 12(a), varied with tip speed from 0.9 to 1.64, but was essentially constant over the entire span at each speed. At 98 percent of design speed, the relative inlet Mach number was lower than predicted (1.43 compared with 1.53) as a result of the lower axial velocity into the rotor as evidenced by the lower-than-estimated weight flow (computed at design speed for Freon-12, 52.3 pounds per second; measured, 46.5 pounds per second).

Both the relative inlet Mach number and relative inlet angle remained unaffected at maximum back pressure, as may be seen from a comparison of figures 11(a) and 12(a) with figures 11(b) and 12(b). This substantiates the constant weight flow as measured by the venturi.

Weight flow.- The exit weight-flow distribution, presented in figure 13 as a nondimensional ratio of the elemental value of $\rho_2 V_{a,2}$ to the average elemental value of $\rho_2 V_{a,2}$, shows that reverse flow occurred at the hub at all speeds for the open throttle condition. The short, vertical tick marks indicate the radial position of the limiting through-flow streamline. The exact reason for this reverse flow is not fully understood. However, it may be attributed to boundary-layer centrifugation and secondary flow effects for the following reason: The static-pressure distribution over the rotor (fig. 10(a)), shows that a large static pressure rise was measured about 2 inches behind the leading edge. The ratio of the maximum to the minimum static pressure of 2.3 indicates the presence of a strong shock within the blading. It is apparent that this shock exists for some reason other than the necessity of balancing the downstream pressure, as evidenced by the subsequent reexpansion within the blade passage. This shock may be caused by the coalesence of compression waves originating at the hub. It cannot be determined whether these compression waves on the hub are caused by the initial area contraction through the first half of the rotor, or by the inward centrifugation of the boundary layer (to be explained subsequently), or, more likely, a combination of the two. In any case, the pressure rise across these compression waves is apparently strong enough to cause separation of the flow on the hub. In addition, the separation on the blade surfaces is increased because of shock boundary-layer interaction and is swept inward adding to the region of separation at the root. The low-energy fluid accumulated at the hub cannot overcome the rising static-pressure gradient which must exist on the rotor hub and a circulatory flow results.

At maximum back pressure, the region of reverse flow increased for tip speeds above 59 percent of design as seen in figure 13(b). This increase is attributed to the existence of a stronger shock within the

blading as evidenced by the higher pressure ratio at maximum throttle in figure 10(a) (2.4 as compared with 2.3). This stronger shock is due to an increased pressure gradient along the hub caused by the upstream propagation of disturbances through the low-energy region.

At 59 percent of design speed, the region of reverse flow disappeared at maximum back pressure. The explanation for this unusual occurrence may be made on the basis of figure 10(b). At the open-throttle condition, the presence of a large pressure ratio within the blading is again indicative of a strong shock which induces separation and a circulatory flow as previously discussed for the near design speed test. However, at maximum throttle, this large pressure ratio and the associated shock are no longer present. The static pressure over the rotor now gradually increases from the rotor leading edge; this indicates that supersonic velocity is never attained within the blading since the relative inlet Mach number is about 0.9, as seen in figure 12.

The inward centrifugation of the boundary layer is a characteristic of rotors turning past axial. Here the tangential component of the absolute exit velocity $V_{u,2}$ is greater than the rotational speed U_2. Therefore, the boundary layer, rotating at U_2, is thrown inward because the static-pressure gradient for simple radial equilibrium, determined from the free-stream conditions, is greater than the centrifugal force acting on a particle in the boundary layer. This is just opposite to the effect in a rotor turning to less than the axial direction where the boundary layer tends to flow outward.

Static-pressure ratio.- The static-pressure distribution at the discharge measuring station is shown in figure 14. For the open throttle condition (fig. 14(a)), the static-pressure rise across the rotor as well as the static-pressure gradient increased with increasing tip speed. At 59 percent of design speed, the rotor produced a static-pressure drop over the entire span, while at 119 percent of design speed, a static-pressure rise was measured over most of the region of through flow with a maximum value of two at the tip. At 98 percent of design speed, the tip section produced a much higher static-pressure ratio than that called for in the design (1.65 as compared with 1.14). This is to be expected in the absence of stators because of the inability of the flow downstream of the rotor to continue in the same plane as the flow path designed through the rotor. The constant slope of the outer casing extending downstream of the rotor constrains the flow and requires a pressure gradient which must be in excess of the design value. It is apparently fortuitous that impulse operation was actually attained so close to the pitch section since the influence of the higher static-pressure gradient in the absence of stators will be propagated upstream into the rotor. In addition, the blockage caused by the region of

reverse flow at the hub also affects the static-pressure level and the variation of flow area will change the radial position at which impulse operation is achieved.

Evidence of the fact that the downstream boundary conditions influenced the flow in the rotor can be seen from figure 15. Here the measured radial pressure gradient at the discharge measuring station is compared with the gradient calculated for simple radial equilibrium $\left(\frac{dp}{dr} = \rho\frac{V_u^2}{r}\right)$. In spite of the fact that the rotor design ignored simple radial equilibrium for spiral flow, the flow actually very nearly attained this condition 3/4 inch behind the rotor over the region of through flow. This could not be achieved in such a short distance behind the rotor without influencing the flow in the rotor.

The effect of maximum throttle on the static-pressure ratio is shown in figure 14(b). The static-pressure ratio increased over the entire span although the radial gradient remained about the same for corresponding speeds as for the open throttle condition. In addition to the increased diffusion in the rotor at maximum throttle causing an increase in the static-pressure ratio, there is a reduction in the effective flow area resulting from the increased region of reverse flow which also causes an increase in static pressure.

Total-pressure ratio and efficiency.- The spanwise variations of total-pressure ratio and efficiency are shown in figures 14 and 16. For open throttle, the peak values of pressure ratio and efficiency occurred at the same radial position at each speed and moved outward toward the tip as the rotational speed was increased. At speeds below design, the peak values occurred near the mean radius; at 98 percent of design speed, the peak total-pressure ratio of 11.8 occurred at a slightly higher radius, and at 119 percent of design speed a peak total-pressure ratio of 26.7 was measured at the tip. As the rotational speed was increased, the total-pressure ratio increased along the entire span while the efficiency increased near the tip but decreased near the pitch. This may be attributed to the fact that at the lower speeds the small static-pressure gradient does not allow the boundary layer at the tip to centrifuge rapidly toward the hub and thus the losses remain at the tip and show up as lower efficiencies. However, as the rotational speed increased, a corresponding increase in static-pressure gradient caused an increase in the inward centrifugation of the boundary layer and carried the losses down further toward the hub. The low efficiencies near the hub at all speeds indicate high losses which are expected from the low-energy circulating flow in that region.

The effect of maximum back pressure on the total-pressure ratio and efficiency can be seen in figures 14(b) and 16(b). At 98 percent and 88 percent of design speed, the total-pressure ratio and efficiency were not affected at the tip section but were reduced at the mean section. This is attributed to the increase in the aforementioned separation which could be centrifuged inward from the tip but not from the mean section because of the increased region of reverse flow. At 59 percent of design speed, the greatest effect of back pressure resulted at the hub because of the disappearance of the reverse flow. At this speed, the total-pressure ratio was nearly uniform over the entire span.

Exit Mach number.- The radial distributions of exit Mach numbers are presented in figure 12. At the lowest speed, for the open throttle condition (fig. 12(a)), the relative exit Mach number over most of the span was larger than the relative inlet Mach number. At the higher speeds, the opposite effect is seen; that is, the relative flow through the rotor was decelerated. At 98 percent of design speed, the relative exit Mach number is below the design value at all radial stations. Since the design values were computed for ideal flow conditions, losses in the rotor would reduce the observed relative discharge Mach number. At the radius which produced impulse operation $\left(r = 0.636 \text{ where } p_2/p_1 = 1.0\right)$, the difference between $M_{2R}(1.33)$ and $M_{1R}(1.44)$ is a measure of the relative total-pressure loss. Thus the decrease in the relative exit Mach number from the mean radius toward the tip as well as toward the root reflects the increased losses indicated by the efficiency distribution.

The absolute exit Mach number increased with increasing rotor speed at all radial stations with the greatest rate of increase occurring at the tip. At 98 percent of design speed, the absolute discharge Mach number varied from 1.95 at the tip to a maximum value of 2.33 near the mean radius. This is considerably lower than the design values due to diffusion as well as the above-mentioned losses in the rotor.

At maximum back pressure, the exit Mach numbers (fig. 12(b)) were reduced at all speeds due to the increased diffusion.

Exit angles.- The radial distributions of the absolute exit angles and the rotor turning angles are presented in figure 11. At open throttle, figure 11(a), the maximum variation of the measured discharge angle with tip speed is about 8° at the section slightly inboard of the mean radius. The maximum radial variation over the region of through flow is about 7° at the low rotational speeds and decreases with increasing rotor speed. At 98 percent of design speed the measured discharge angle is about 2° higher at the tip and 7° lower at the pitch than estimated. The radial distribution of turning angle shows a 5° change with rotor

speed at the mean radius and a maximum variation of 13° at the tip. At 98 percent of design speed, the rotor produced nearly constant turning of about 105° over the region of through flow. This is very close to the design value at the tip and about 9° lower than design at the pitch.

At maximum throttle (fig. 11(b)), the absolute exit angle was practically unaffected over the region of through flow at the higher speeds. At 59 percent of design speed, the measured discharge angle was about 5° higher over the outer half of the span but considerably lower near the hub. The turning angle was decreased by throttling by about 5° over most of the region of through flow for the higher speeds. At the lowest speed, the turning was increased at the tip but remained about the same at the pitch.

ROTOR WITH GUIDE VANES IN PRESENCE OF STATORS

Because the design philosophy of restricting the flow to a plane (rather than the usual spiral path about the axis of rotation) was not carried downstream of the rotor, it was realized that placing stators very close to the rotor would be necessary to prevent the establishment of a strong static-pressure gradient downstream of the rotor. In order to verify experimentally the design method, it was believed essential to avoid the influence which such a pressure gradient would have upon the flow within and leaving the rotor. Therefore, initial tests of a preliminary nature were made with the set of sheet-metal stators previously described. These stators were not designed to recover a significant portion of the kinetic energy imparted by the rotor, but were intended only to avoid the strong static-pressure gradient.

Tests with these stators were made prior to those with the rotor alone. The stators were located $1\frac{3}{16}$ inches behind the rotor to permit the installation of instrumentation. The problems of flow measurements previously discussed under the section entitled "Procedure" were further increased because of the influence of the stators upon the measurements of the flow parameters. At the time these tests were run, torque measurements were not available as a check upon the other methods of obtaining the power input. The efficiencies determined from momentum and temperature conditions differed by about 9 percent with the temperature rise efficiency consistently higher. In addition, the rotor exit weight flow was consistently about 10 percent lower than the rotor inlet weight flow. For these reasons, the results obtained from these tests with the stators in place are questionable. Nevertheless, interesting and instructive results were obtained concerning the performance of this rotor in the presence of these stators.

Tests of the rotor—guide-vane combination with the sheet-metal stators were made over an equivalent tip-speed range of 65 percent to 119 percent of design speed at open and maximum throttle. The static and total pressure survey measurements appeared to be more consistent at 91 percent of design speed at open throttle than at any other speed and only these results are presented herein. It should be noted that the results of the tests at other speeds and throttle conditions show similar trends.

The major effect of the stators upon the performance of the rotor was to eliminate the separated, recirculating flow at the rotor hub at all speeds and throttle conditions. In addition, the flow leaving the rotor had a much more uniform radial distribution of angle, Mach number, total-pressure ratio, mass flow, and efficiency, as seen in figure 17. Another significant effect of the stators was to reduce the shock strength within the rotor at open throttle as indicated by the static-pressure distribution along the outer casing in figure 18. These effects of the presence of the stators on the rotor performance are attributed to a reduction of the static pressure at the rotor exit. The mechanism by which this is accomplished may be explained as follows: A separated, recirculating flow, as in the case of the rotor operating without stators, would result in high positive incidence angles on the stators near the hub. These high incidence angles would give rise to expansion waves at the leading edge of the stator which would propagate upstream into the rotor thereby increasing the velocity and decreasing the static pressure. The pressure gradient along the hub is therefore reduced sufficiently to permit attached flow, as evidenced in figure 17(d). The elimination of the recirculatory flow increases the effective flow area at the rotor exit; this increases the Mach number and therefore reduces the static pressure level from hub to tip. The maximum static pressure measured along the outer casing at maximum throttle was equal to that measured with the rotor alone but was not located as far upstream (fig. 18). The high static-pressure rise within the rotor is due to the inability of the stators to hold a normal shock at this throttle condition.

In spite of the radial differences observed in all the measured flow parameters when operating with and without stators, the overall performance of the rotor remained about the same. The rotor in the presence of the stators produced a total-pressure ratio of 7.3 with an efficiency (based upon momentum considerations) of 82 percent and an equivalent weight flow of 45.8 pounds per second of Freon-12 at an equivalent tip speed in Freon-12 of 570 feet per second. These values compare with 7.6, 86, and 45.4, respectively, for the rotor without stators. However, as indicated previously, these data are not sufficiently accurate to permit drawing conclusions from these values.

It is believed that the stators permitted the flow in the rotor to approach the conditions postulated in the design philosophy. Although the radial static-pressure gradient (fig. 17(c)) is larger than the gradient specified in the design, the difference from hub to tip is about $0.7p_1$ rather than the value of $2.06p_1$ calculated for spiral flow about the axis of rotation. The flow leaving the rotor was sufficiently uniform in angle, Mach number, and total pressure to make possible efficient recovery of the high kinetic energy if suitable stators were used.

ROTOR ALONE

Overall Performance

In order to gain further insight into the performance of rotors of this type, the guide vanes were removed and the rotor was tested as a separate component. The overall performance of the rotor alone is presented in figure 19 in terms of total-pressure ratio, efficiency, and equivalent weight flow as functions of equivalent tip speed.

Open throttle.- For the open-throttle condition, removal of the guide vanes had no effect on the total-pressure ratio and efficiency at 58 percent of design speed. However, at higher speeds, the total-pressure ratio was decreased and the efficiency was increased by removing the guide vanes. At design speed, the total-pressure ratio of 9.1 was 5 percent less and the efficiency of 89.5 was 4 percent greater than that measured with guide vanes; at 112 percent of design speed, the total-pressure ratio of 13.2 was 12 percent less and the efficiency of 88.5 was 3 percent higher than that obtained with the rotor—guide-vane combination. This decrease in total-pressure ratio is expected since removal of the guide vanes, which were designed to turn against the direction of rotation, reduces the work input. The increase in efficiency is attributed to the elimination of guide-vane losses and a reduction in friction drag and shock losses due to a decrease in the average relative inlet Mach number.

At all speeds, removal of the guide vanes decreased the equivalent weight flow from 3.5 to 5 percent. For supersonic compressors, the relative air inlet angle remains approximately the same irrespective of guide vane turning. Therefore, for the same rotational speed, removal of the guide vanes which turned against the direction of rotation must decrease the axial velocity and thus decrease the weight flow.

Effect of back pressure.- As in the case of the rotor—guide-vane combination, the total-pressure ratio and efficiency remained constant with increasing back pressure until the maximum throttle point was

reached. At maximum throttle, the total-pressure ratio and efficiency were reduced by about 16 percent and 6 percent, respectively. Back pressure had no effect on the weight flow at the higher speeds but at 58 percent of design speed, the weight flow was reduced about 5.5 percent. At the lower speeds, removing the guide vanes apparently reduces the relative inlet Mach number sufficiently to allow the downstream disturbances to be felt ahead of the rotor.

The effect of back pressure on the static-pressure distribution along the outer casing is shown in figure 20 for 99 percent and 58 percent of design speed. At 99 percent of design speed (fig. 20(a)) the static pressure ahead of the rotor remained constant with back pressure, but at 58 percent of design speed (fig. 20(b)) the upstream static pressures were increased at maximum throttle, indicating a decrease in weight flow.

Blade-Element Peformance

Radial distributions of several rotor parameters at several tip speeds are presented in figures 21 to 25 for the open- and maximum-throttle conditions.

Inlet conditions.- The radial variations of the relative inlet angles are presented in figure 21 for the rotor alone operating at several tip speeds. For the open-throttle condition, removing the guide vanes reversed the slope of the spanwise variation of the relative inlet angles with the smallest changes in angle occurring at the mean section. The large angle change which occurred at the root section might be expected since the guide-vane turning was 27.6° at that station. However, at the tip section, where the guide-vane turning was 0°, no change in inlet angle would be expected on a two-dimensional basis. Therefore, the change at the tip caused by the removal of the guide vanes (as much as 4.5° at 88 percent of design speed) must be a result of three-dimensional wave effects upstream of the rotor.

The relative inlet Mach numbers, presented in figure 22, show that, for the open-throttle condition, removing the guide vanes reduced the inlet Mach number at the root but had little effect at the tip. At 99 percent of design speed the relative inlet Mach number varied from 1.1 at the root to 1.4 at the tip.

The relative inlet Mach number (fig. 22(b)) remained unaffected with back pressure at each speed. The relative inlet angle (fig. 21(b)) remained constant with increasing throttle at the higher speeds, varying only at 58 percent of design speed.

Exit conditions.- In general, the exit-flow parameters all show the same trends as those obtained for the rotor operating with guide vanes. The region of reverse flow, seen in the weight-flow distributions (fig. 23) increased slightly at all speeds for the open-throttle condition, and at maximum throttle the circulatory flow again disappeared only at 58 percent of design speed. The static-pressure distributions along the outer casing (fig. 20) indicate that the same explanation applies for the presence, and disappearance, of this circulatory flow as for the rotor—guide-vane configuration.

The static-pressure ratio (fig. 24) was reduced for all speeds at both open and maximum throttle, except at 58 percent of design speed where removal of the guide vanes had no effect on the static-pressure ratio over the entire span. The peak values of total-pressure ratio (fig. 24), efficiency (fig. 25), and Mach number (fig. 22) occurred at a radius slightly inboard of that measured for the rotor with guide vanes. The turning angles and absolute exit angles (fig. 21) were approximately 2° lower than those obtained with guide vanes.

MODIFIED ROTOR HUB CONTOUR

In an effort to eliminate the region of reverse flow of the rotor alone, the rotor-hub contour was modified by smoothly building up the rear $1\frac{1}{2}$ inches with balsa inserts to increase the exit hub-tip radius-ratio from 0.795 to 0.825. The results were obtained only for the rotor alone operating at open throttle over a speed range of 86 percent to 112 percent of design because during subsequent tests some of the balsa inserts flew off and testing was discontinued.

A comparison of the overall performance (fig. 19) shows that modifying the hub had no effect on the total-pressure ratio but decreased the efficiency about 3 percent at all speeds. The weight flow remained the same at speeds above design but was reduced slightly at speeds below design.

The static-pressure distribution along the outer casing for 99 percent of design speed shown in figure 26 was obtained from a linear interpolation between 96 percent and 102 percent of design speed tests. A comparison of the static pressures along the outer casing for the original and modified hub contours (fig. 26) indicates the flow within the rotor was affected by the addition of balsa at the hub.

Radial variations of several rotor parameters at several speeds for the rotor with modified hub contour are presented in figures 27 to 30. In general, the distribution of Mach numbers, angles, pressure ratio,

and efficiency remained about the same over the region of through flow as those obtained with the original rotor-hub contour. The exit weight-flow distribution (fig. 30) shows that increasing the contraction ratio across the rotor decreased the region of circulatory flow only slightly at 112 percent of design speed but almost completely eliminated it at 86 percent of design speed.

From the results of the rotor with contracted exit area, it would appear that a further reduction in exit area would result in the elimination of the circulatory flow at speeds higher than 86 percent of design. However, the starting contraction ratio limits the amount of contraction possible. The modified hub contour resulted in an area contraction of about 5 percent whereas the starting contraction ratio for a Mach number of 1.55 (expansion waves due to the 5° positive angle of attack would increase the relative inlet Mach number of 1.42 which was obtained for rotor operating with guide vanes at design speed) allows an area contraction of 14 percent. Although the exit contraction ratio could therefore be further increased, it was felt that the thick balsa inserts would not adhere to the rotor at design speed and further tests were not made.

SUMMARY OF RESULTS

A 16-inch tip-diameter impulse-type supersonic compressor having a mean rotor turning of 114° was designed and tested with Freon-12 as the test medium. Serious difficulties in obtaining accurate measurements were encountered in the presence of stator blades. The measurements taken during tests without stators are believed to be reliable. The results of this investigation are summarized as follows:

1. At the design speed of 626 feet per second in Freon-12 (equivalent air value, 1,370 feet per second) and open throttle condition, the rotor operating with guide vanes produced a total-pressure ratio of 9.6 and an efficiency of 85.5 percent with a weight flow of 46.7 pounds per second of Freon-12. Without guide vanes the values were 9.2, 89.2, and 44.4, respectively.

2. The weight flow was independent of back pressure at all speeds with and without guide vanes. At maximum throttle the total-pressure ratio was decreased by about 18 percent.

3. The average absolute discharge Mach number at design speed was about 2.1 at an average angle of about 65°.

4. At all speeds tested, a region of separated, recirculating flow was measured at the hub downstream of the rotor probably as a result of

the inward centrifugation of the boundary layer in conjunction with a rising pressure gradient along the hub contour.

5. Increasing the exit hub-tip radius ratio from 0.795 to 0.825 by building up the hub with balsa almost completely eliminated the reverse flow at the hub at 86 percent of design speed, but had little effect on the region of separation at higher speeds. The modified hub contour had essentially no effect on the overall performance of the rotor.

6. The presence of sheet-metal stator blades behind the rotor eliminated the recirculating flow at the hub at all speeds. This result is believed to be due to reduced downstream static pressure caused by expansion waves from the leading edges of the stator blades. The exit flow parameters resulting from the elimination of separation were more nearly uniform than those obtained from the rotor alone, although the overall performance remained essentially the same.

Langley Aeronautical Laboratory,
National Advisory Committee for Aeronautics,
Langley Field, Va., September 12, 1956.

REFERENCES

1. Wright, Linwood C., and Klapproth, John F.: Performance of Supersonic Axial-Flow Compressors Based on One-Dimensional Analysis. NACA RM E8L10, 1949.

2. Erwin, John R., Wright, Linwood C., and Kantrowitz, Arthur: Investigation of an Experimental Supersonic Axial-Flow Compressor. NACA RM L6J01b, 1946.

3. Johnsen, Irving A., Wright, Linwood C., and Hartmann, Melvin J.: Performamce of 24-Inch Supersonic Axial-Flow Compressor in Air. II - Performance of Compressor Rotor at Equivalent Tip Speeds From 800 to 1765 Feet per Second. NACA RM E8G01, 1949.

4. Boxer, Emanuel, and Erwin, John R.: Investigation of a Shrouded and Unshrouded Axial-Flow Supersonic Compressor. NACA RM L50G05, 1950.

5. Liccini, Luke L.: Analytical and Experimental Investigation of 90° Supersonic Turning Passages Suitable for Supersonic Compressors or Turbines. NACA RM L9G07, 1949.

6. Ferri, Antonio: Preliminary Analysis of Axial-Flow Compressors Having Supersonic Velocity at the Entrance of the Stator. NACA RM L9G06, 1949.

7. Boxer, Emanuel, Sterrett, James R., and Wlodarski, John: Application of Supersonic Vortex-Flow Theory to the Design of Supersonic Impulse Compressor- or Turbine-Blade Sections. NACA RM L52B06, 1952.

8. Goldberg, Theodore J., Boxer, Emanuel, and Bernot, Peter T.: Experimental Investigation of an Axial-Flow Supersonic Compressor Having Rounded Leading-Edge Blades With an 8-Percent Mean Thickness-Chord Ratio. NACA RM L53G16, 1953.

9. Zimney, Charles M., and Lappi, Viola M.: Data for Design of Entrance Vanes From Two-Dimensional Tests of Airfoils in Cascade. NACA WR L-188, 1945. (Formerly NACA ACR L5F18.)

10. NACA Subcommittee on Compressors: Standard Procedures for Rating and Testing Multistage Axial-Flow Compressors. NACA TN 1138, 1946.

11. Huber, Paul W., and Kantrowitz, Arthur: A Device for Measuring Sonic Velocity and Compressor Mach Number. NACA TN 1664, 1948. (Supersedes NACA RM L6K14.)

12. Ullman, Guy N., Hartmann, Melvin J., and Tysl, Edward R.: Experimental Investigation of a 16-Inch Impulse-Type Supersonic-Compressor Rotor. NACA RM E51G19, 1951.

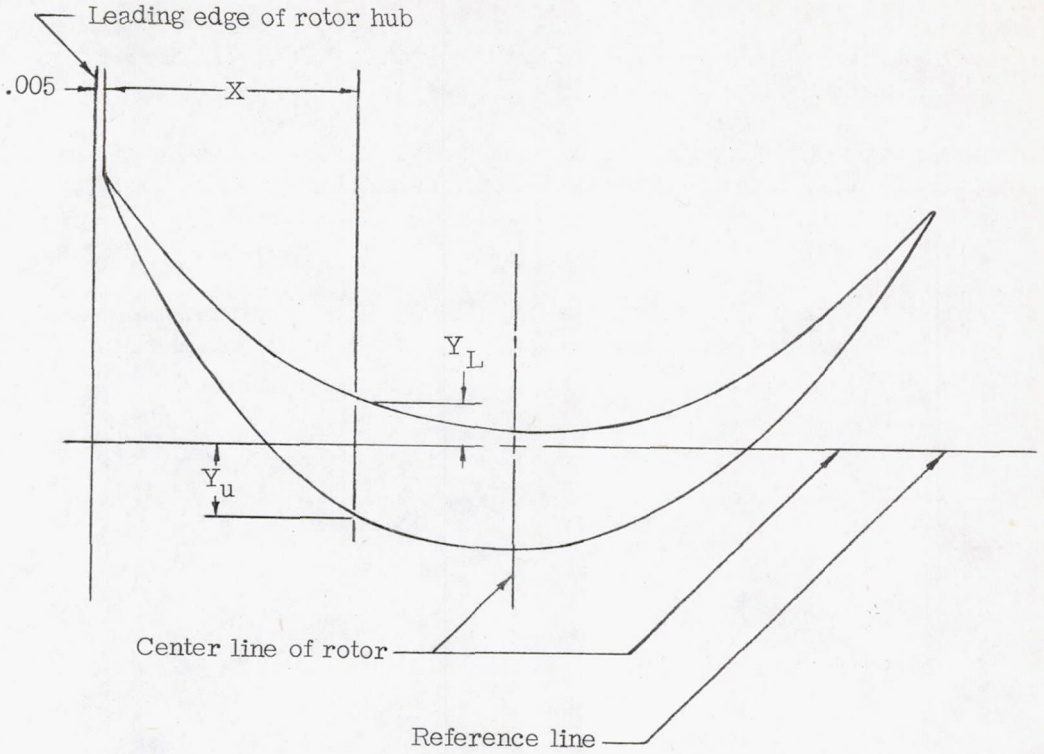
13. Jacklitch, John J., Jr., and Hartmann, Melvin J.: Investigation of 16-Inch Impulse-Type Supersonic Compressor With Rotor Turning Past Axial Direction. NACA RM E53D13, 1953.

14. Tysl, Edward R., Klapproth, John F., and Hartmann, Melvin J.: Investigation of a Supersonic-Compressor Rotor With Turning to Axial Direction. I - Rotor Design and Performance. NACA RM E53F23, 1953.

15. Goldstein, Arthur W., and Schacht, Ralph L.: Performance of a Swept Leading Edge Rotor of the Supersonic Type With Mixed Flow. NACA RM E52K03, 1953.

TABLE I.- BLADE ORDINATES

(a) Root section (6-inch radius)

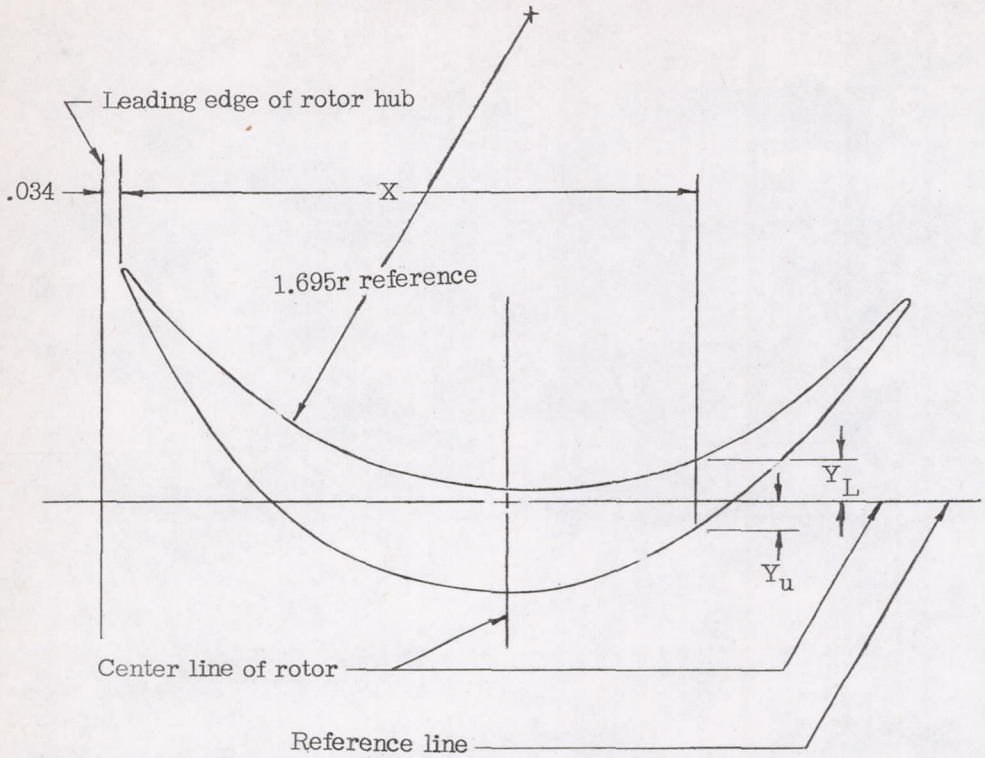


All dimensions in inches

X	Y_U	Y_L
0	-0.879	-0.879
.015	-.847	-.894
.049	-.780	-.846
.083	-.720	-.800
.150	-.599	-.703
.218	-.476	-.609
.285	-.353	-.527
.420	-.147	-.395
.555	.008	-.292
.690	.116	-.216
.825	.202	-.160
1.095	.323	-.075
1.365	.355	-.032
1.437	----	-.030
1.635	.322	-.047
1.905	.193	-.127
2.175	-.042	-.259
2.445	-.360	-.462
2.580	-.542	-.607
2.715	-.749	-.790
2.730	-.775	-.775

TABLE I.- BLADE ORDINATES - Continued

(b) Pitch section (7-inch radius)

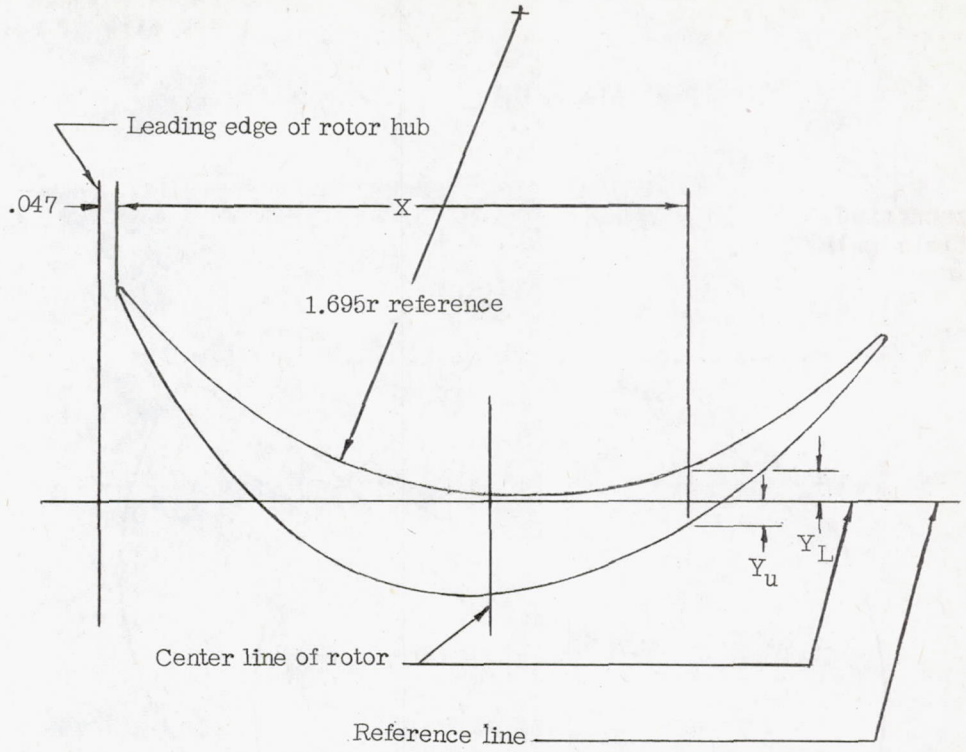


All dimensions in inches

X	Y_U	Y_L
0	-0.792	-0.792
.015	-.763	-.807
.049	-.706	-.777
.083	-.650	-.734
.150	-.541	-.654
.218	-.430	-.574
.285	-.319	-.505
.420	-.139	-.389
.555	.020	-.292
.690	.144	-.215
.825	.213	-.155
1.095	.302	-.076
1.365	.328	-.044
1.419	.3275	-.042
1.635	.282	-.058
1.905	.150	-.118
2.175	-.040	-.230
2.445	-.298	-.411
2.580	-.460	-.534
2.715	-.645	-.683
2.730	-.668	-.668

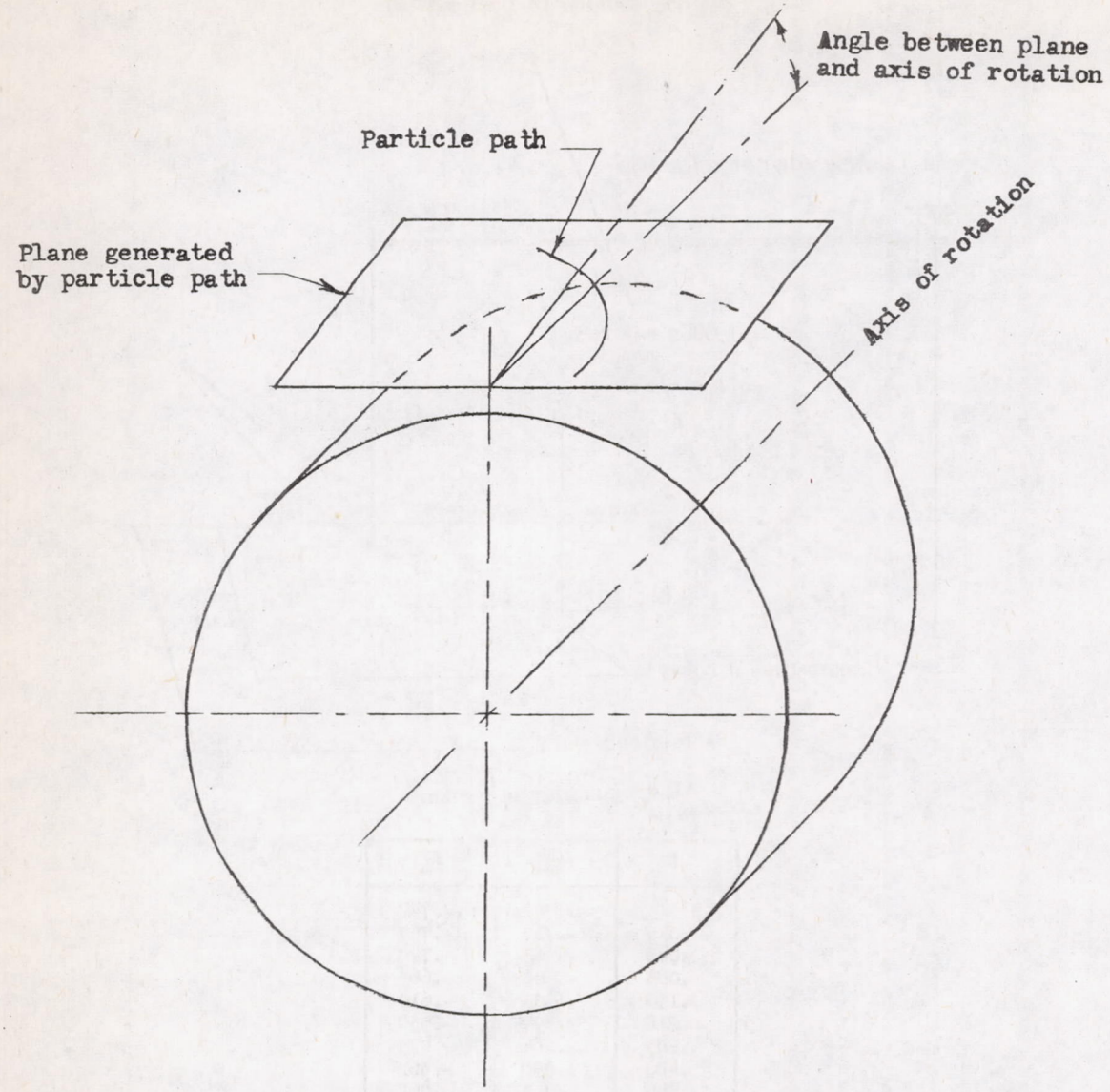
TABLE I.- BLADE ORDINATES - Concluded

(c) Tip section (8-inch radius)



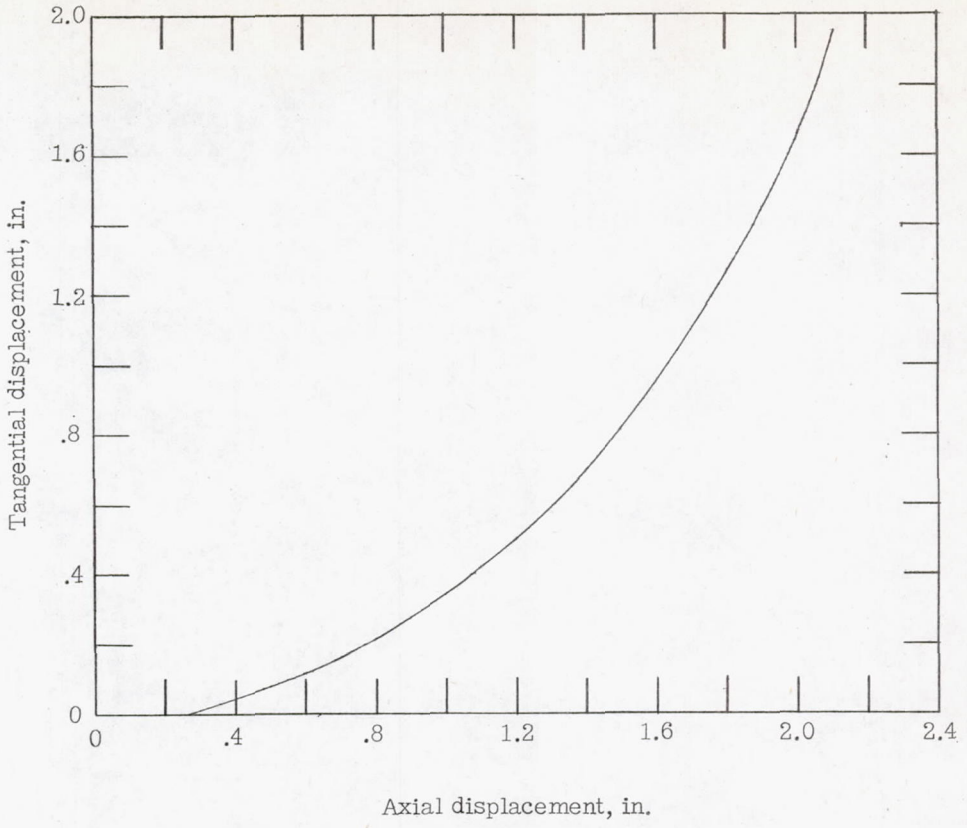
All dimensions in inches

X	Y_U	Y_L
0	-0.742	-0.742
.015	-.717	-.757
.049	-.663	-.722
.083	-.608	-.683
.150	-.503	-.610
.218	-.394	-.539
.285	-.284	-.475
.420	-.098	-.362
.555	.053	-.264
.690	.174	-.190
.825	.254	-.134
1.095	.316	-.055
1.245	.332	-----
1.365	.323	-.021
1.435	----	-.019
1.635	.258	-.030
1.905	.145	-.086
2.175	-.033	-.188
2.445	-.272	-.350
2.580	-.411	-.463
2.715	-.562	-.597
2.730	-.582	-.582

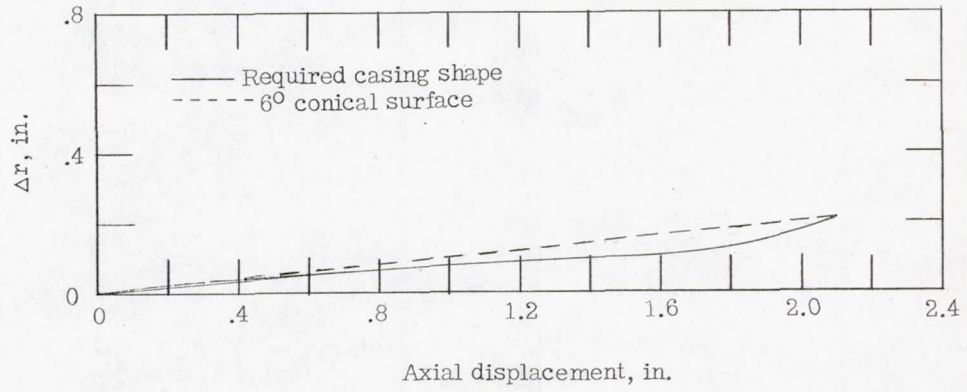


(a) Schematic diagram illustrating a flow plane generated by a particle path.

Figure 1.- Concept of particle flow in a plane employed in the design of the 16-inch impulse-type supersonic compressor investigated herein.

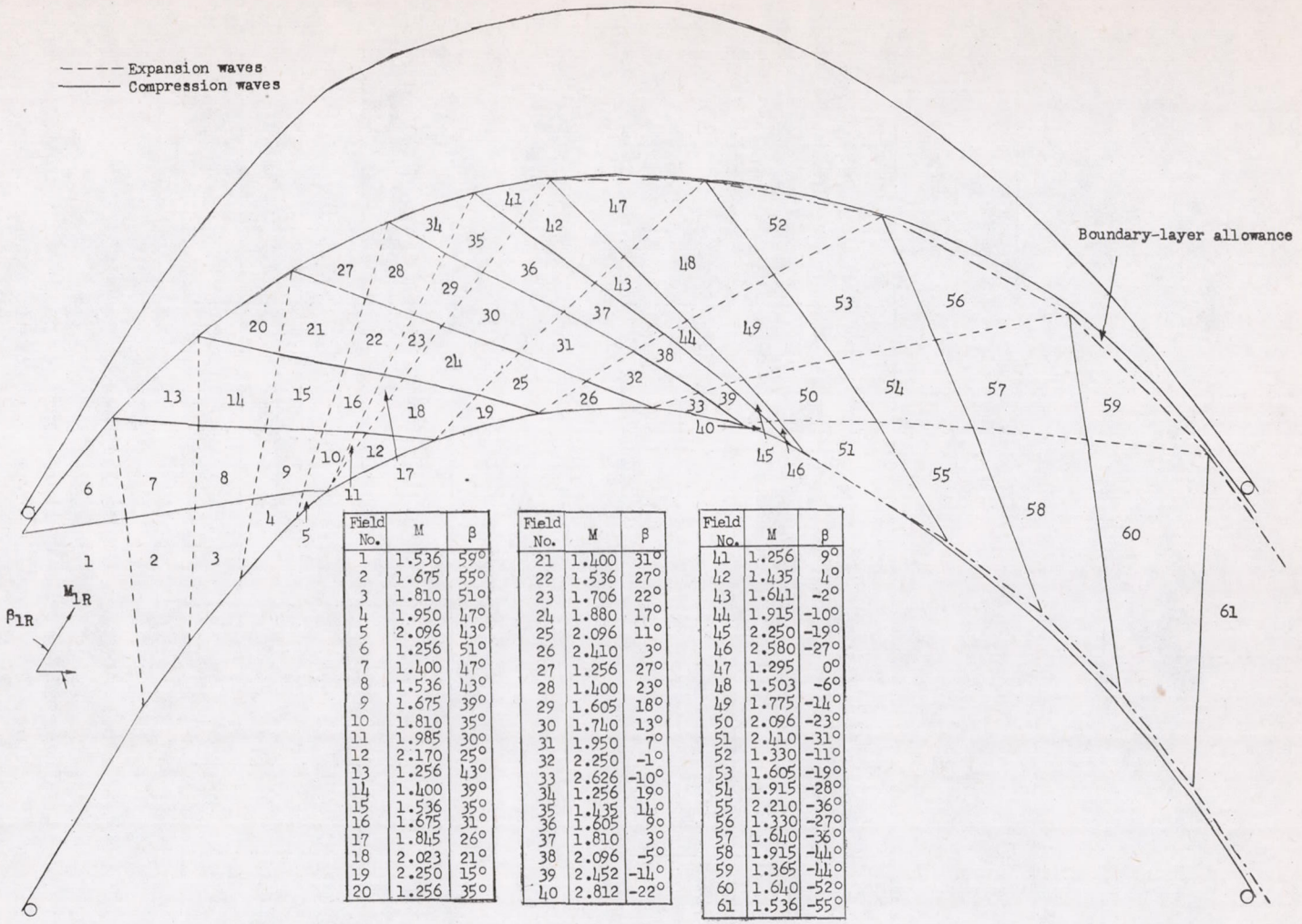


(b) Displacement curve of mean streamline particle path for the tip section.



(c) Mean streamline particle path in meridional plane for the tip section.

Figure 1.- Concluded.

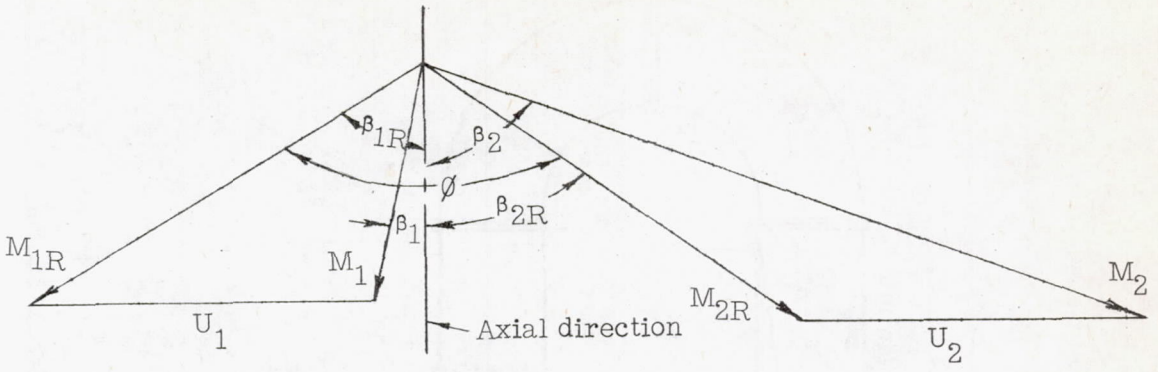


Field No.	M	β
1	1.536	59°
2	1.675	55°
3	1.810	51°
4	1.950	47°
5	2.096	43°
6	1.256	51°
7	1.400	47°
8	1.536	43°
9	1.675	39°
10	1.810	35°
11	1.985	30°
12	2.170	25°
13	1.256	43°
14	1.400	39°
15	1.536	35°
16	1.675	31°
17	1.845	26°
18	2.023	21°
19	2.250	15°
20	1.256	35°

Field No.	M	β
21	1.400	31°
22	1.536	27°
23	1.706	22°
24	1.880	17°
25	2.096	11°
26	2.410	3°
27	1.256	27°
28	1.400	23°
29	1.605	18°
30	1.740	13°
31	1.950	7°
32	2.250	-1°
33	2.626	-10°
34	1.256	19°
35	1.435	14°
36	1.605	9°
37	1.810	3°
38	2.096	-5°
39	2.452	-14°
40	2.812	-22°

Field No.	M	β
41	1.256	9°
42	1.435	4°
43	1.641	-2°
44	1.915	-10°
45	2.250	-19°
46	2.580	-27°
47	1.295	0°
48	1.503	-6°
49	1.775	-14°
50	2.096	-23°
51	2.410	-31°
52	1.330	-11°
53	1.605	-19°
54	1.915	-28°
55	2.210	-36°
56	1.330	-27°
57	1.640	-36°
58	1.915	-44°
59	1.365	-44°
60	1.640	-52°
61	1.536	-55°

Figure 2.- Blade shape of tip section showing two-dimensional characteristic network and allowance for boundary layer.



r_1, ft	r_2, ft	M_1	β_1, deg	M_{1R}	β_{1R}, deg	M_{2R}	β_{2R}, deg	M_2	β_2, deg	p_2/p_1	P_2/P_1
0.667	0.690	0.800	0	1.53	-58.4	1.43	48.5	2.58	68.4	1.14	14.6
.583	.608	.803	-12.3	1.53	-59.1	1.53	55.2	2.60	70.3	1.00	13.0
.500	.542	.822	-27.6	1.54	-61.9	1.65	59.1	2.64	71.3	.85	11.7

(a) Original air design; $\gamma = 1.4$.

r_1, ft	r_2, ft	M_1	β_1, deg	M_{1R}	β_{1R}, deg	M_{2R}	β_{2R}, deg	M_2	β_2, deg	p_2/p_1	P_2/P_1
0.667	0.690	0.800	0	1.53	-58.4	1.44	48.5	2.60	68.5	1.14	19.1
.583	.608	.803	-12.3	1.53	-59.1	1.53	55.2	2.60	70.4	1.00	16.7
.500	.542	.820	-27.6	1.54	-61.9	1.63	59.1	2.61	71.3	.87	14.4

(b) Estimated conversion to Freon-12; $\gamma = 1.125$.

Figure 3.- Velocity diagram for the design conditions in air and conversion to Freon-12 values for impulse-type supersonic compressor.

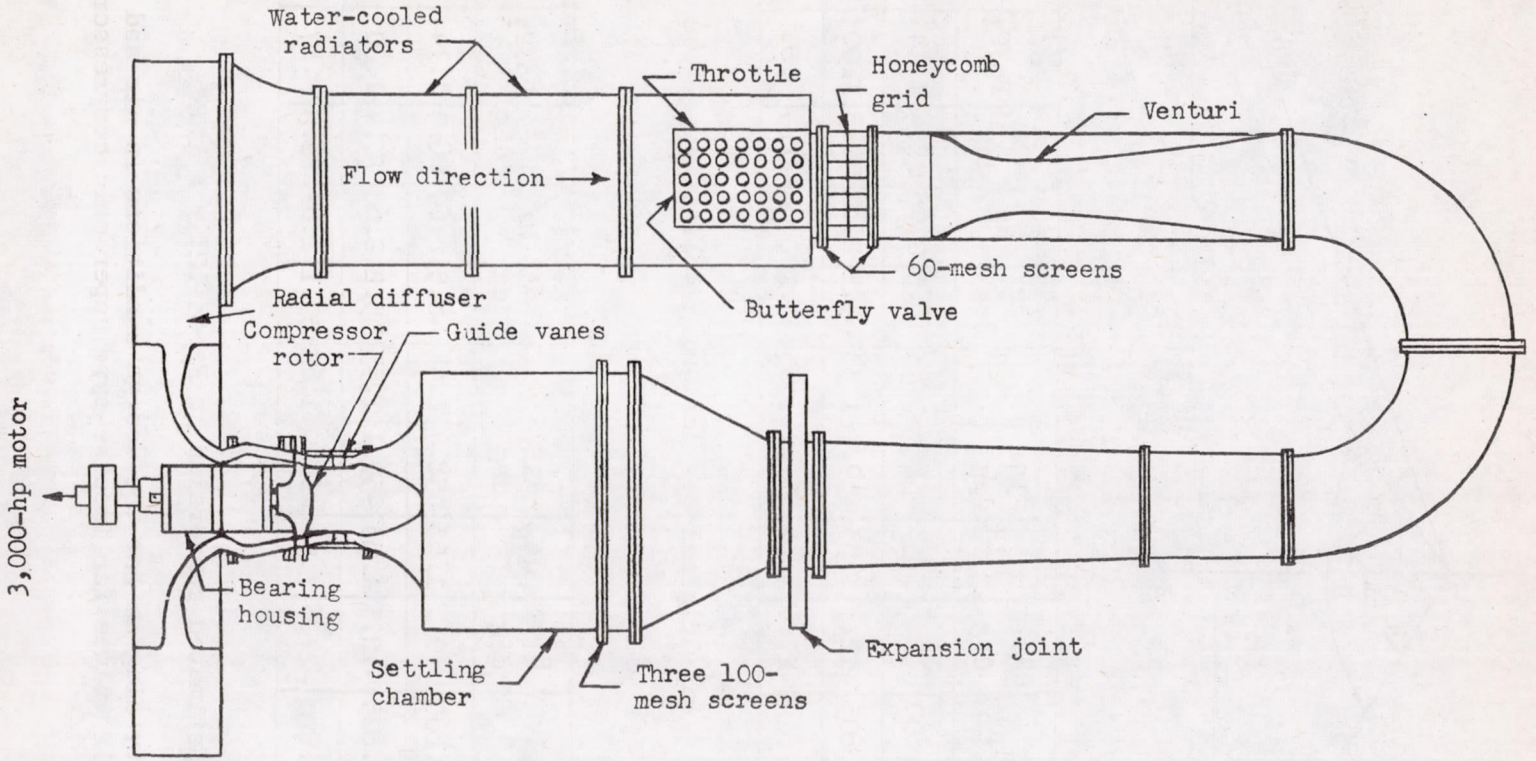


Figure 4.- Arrangement of supersonic-compressor test rig.

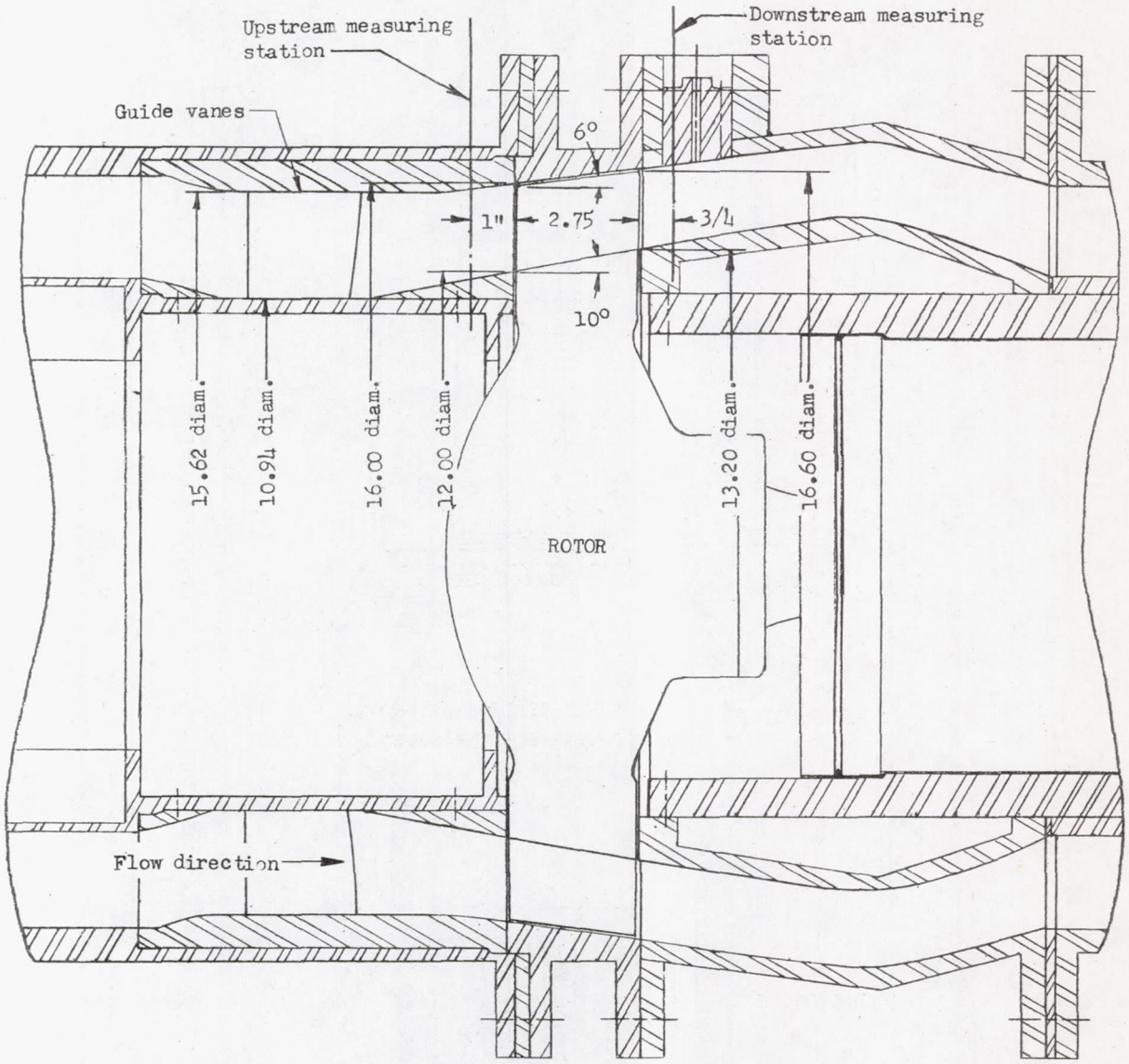
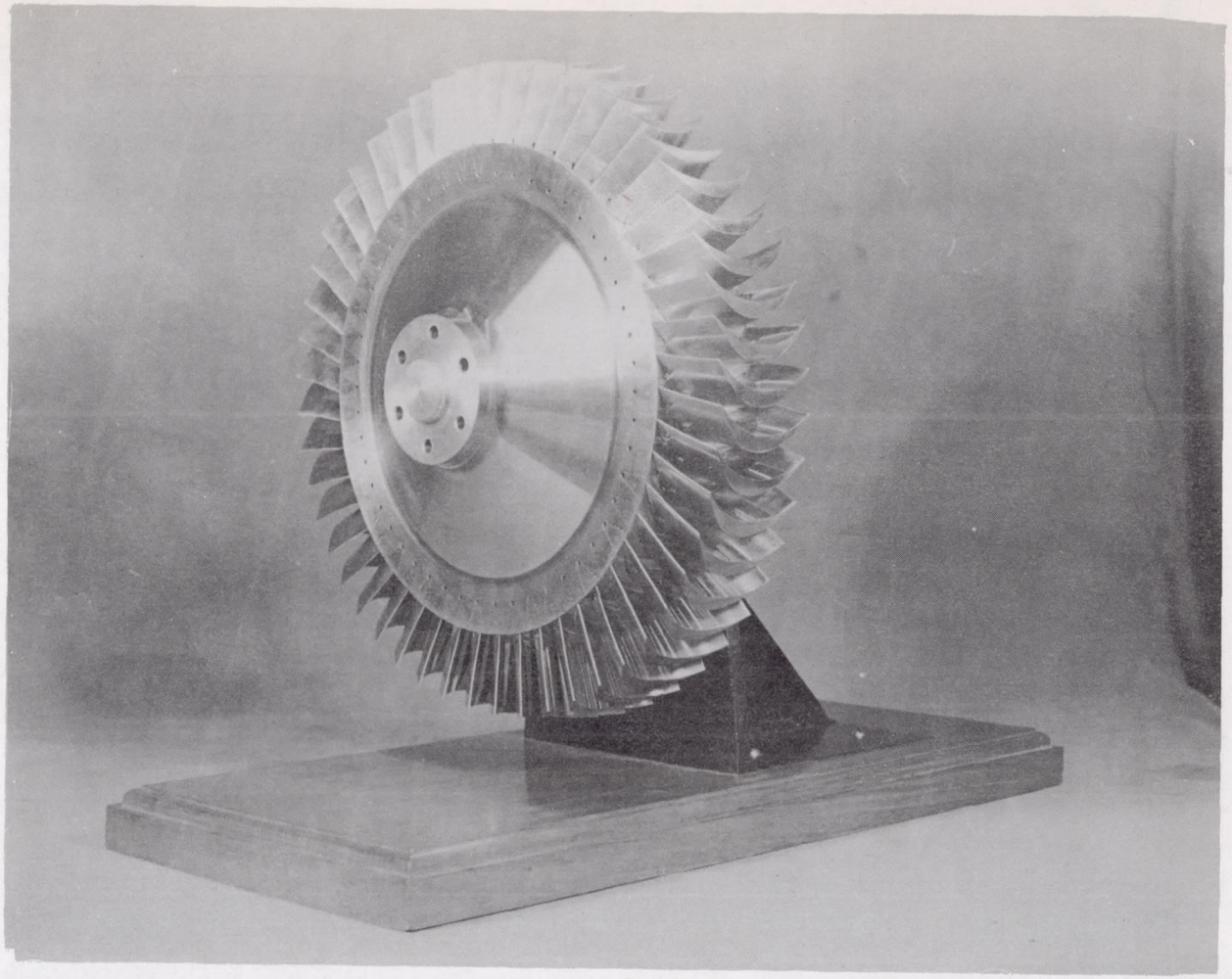


Figure 5.- Sectional view of test section of supersonic-compressor test rig. All dimensions are in inches.



L-63387

Figure 6.- Three-quarter view of 16-inch impulse-type supersonic-compressor test rotor.

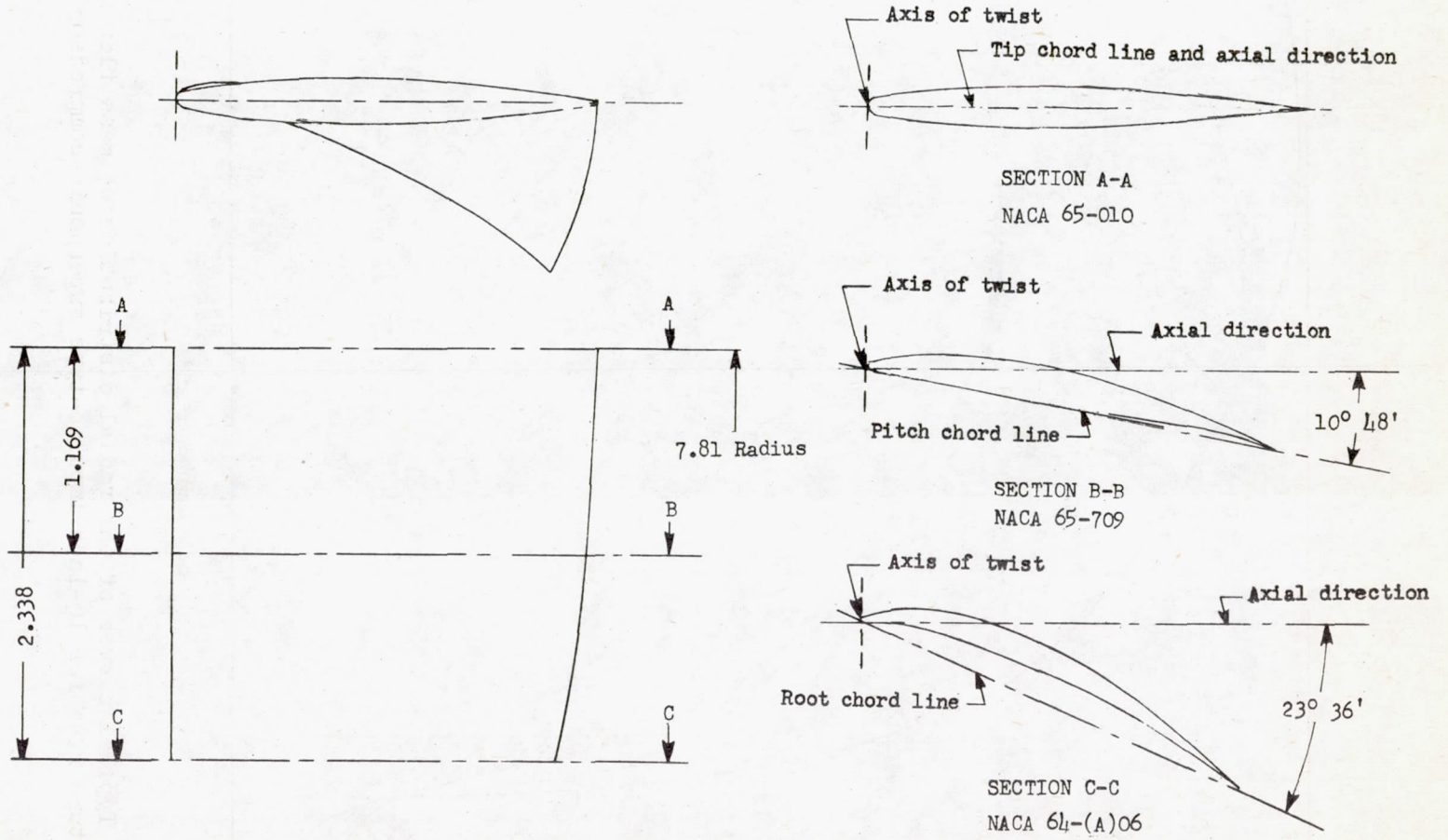


Figure 7.- Guide-vane details. All dimensions are in inches.

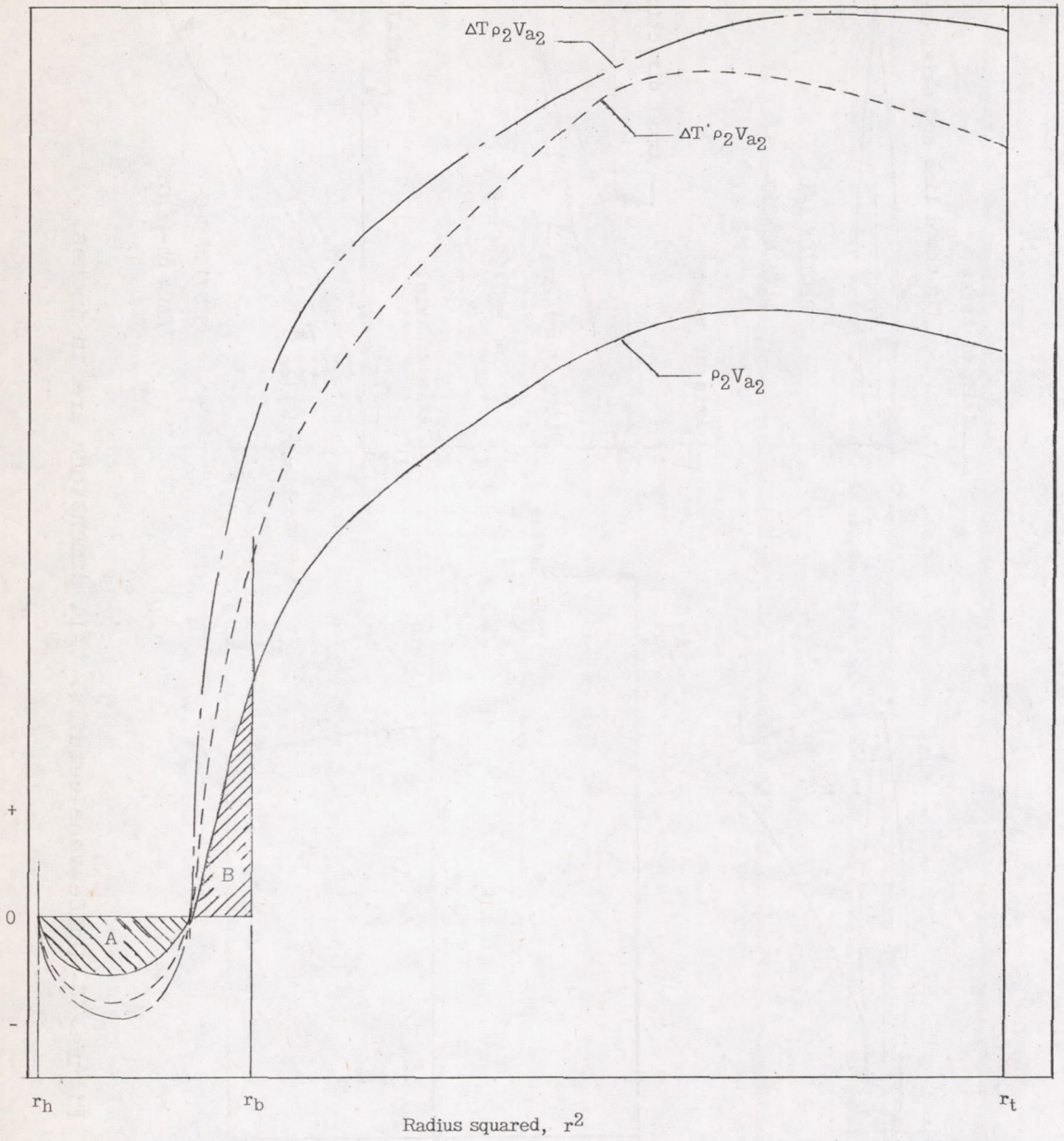


Figure 8.- Typical curves of the radial distribution of mass flow and temperature rise for 16-inch impulse-type supersonic-compressor test rotor.

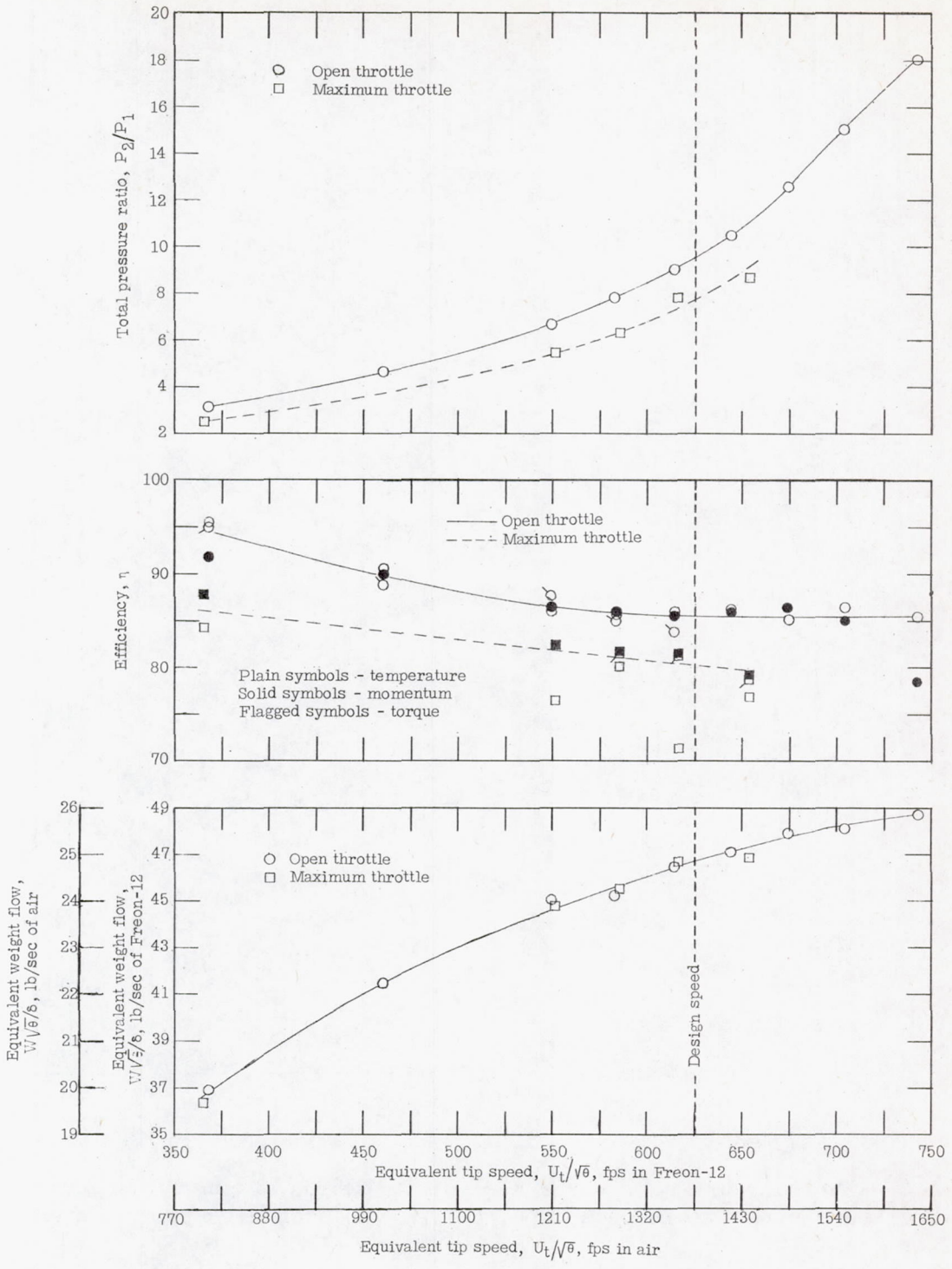
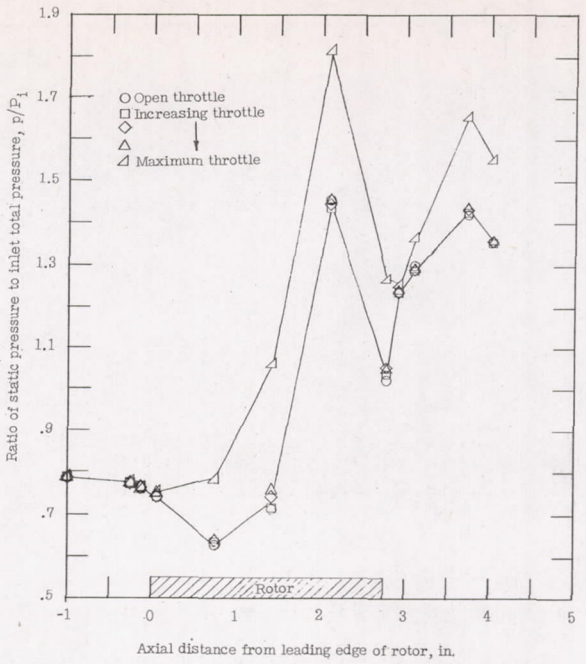
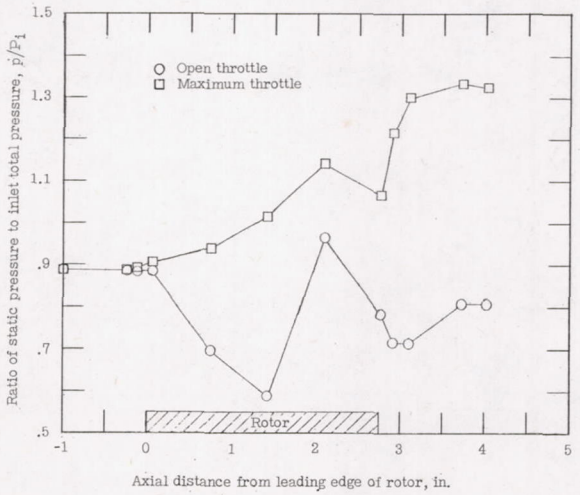


Figure 9.- Rotor characteristics with guide vanes.

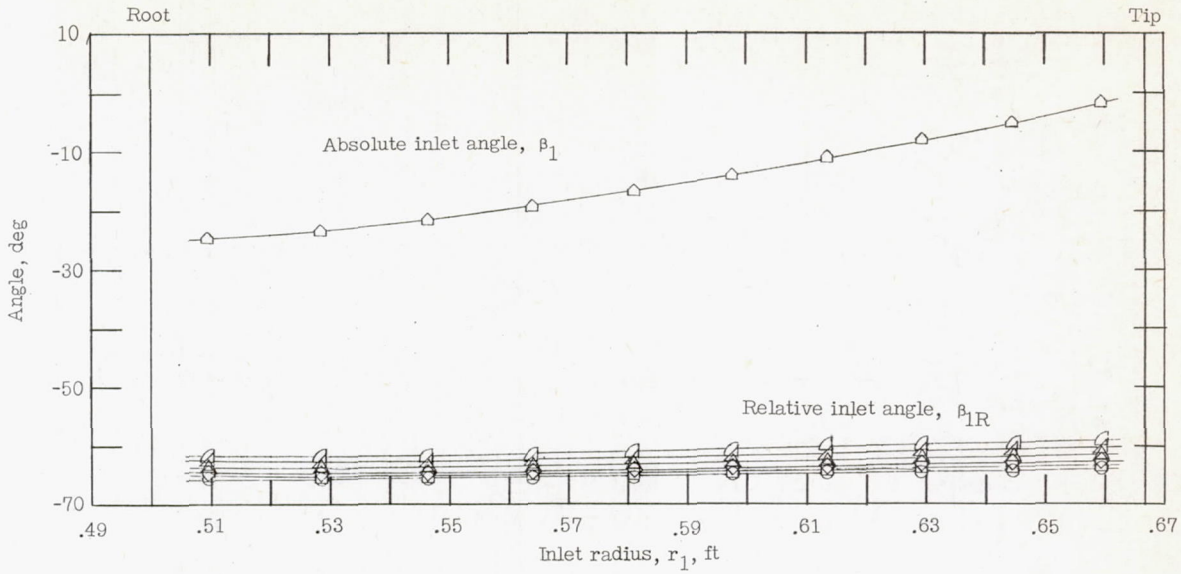


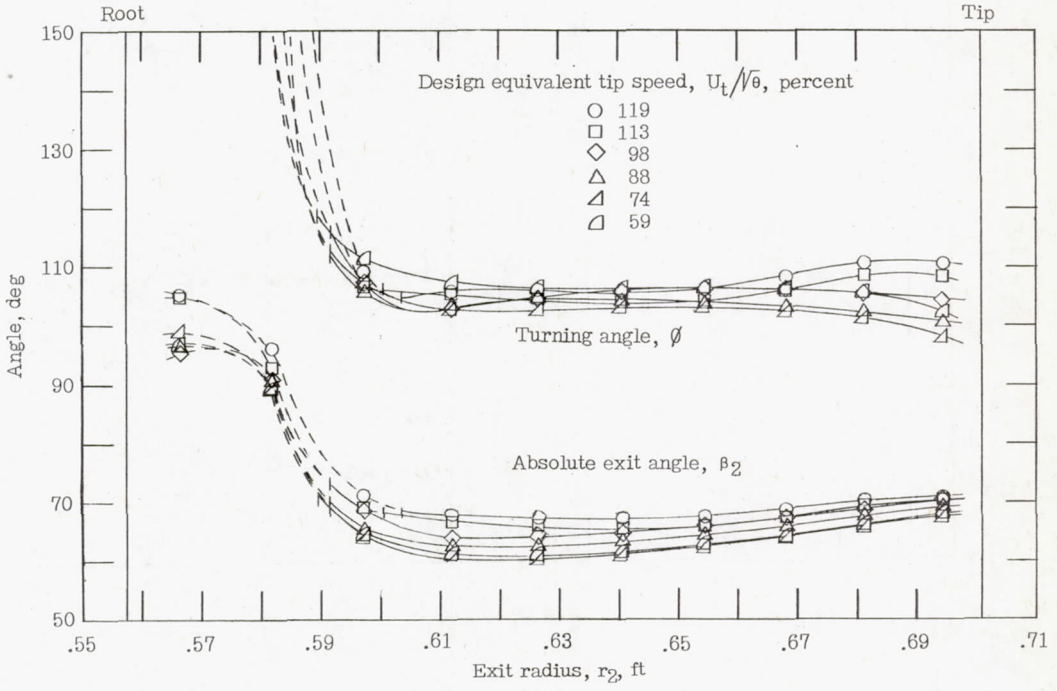
(a) 98 percent of design speed.



(b) 59 percent of design speed.

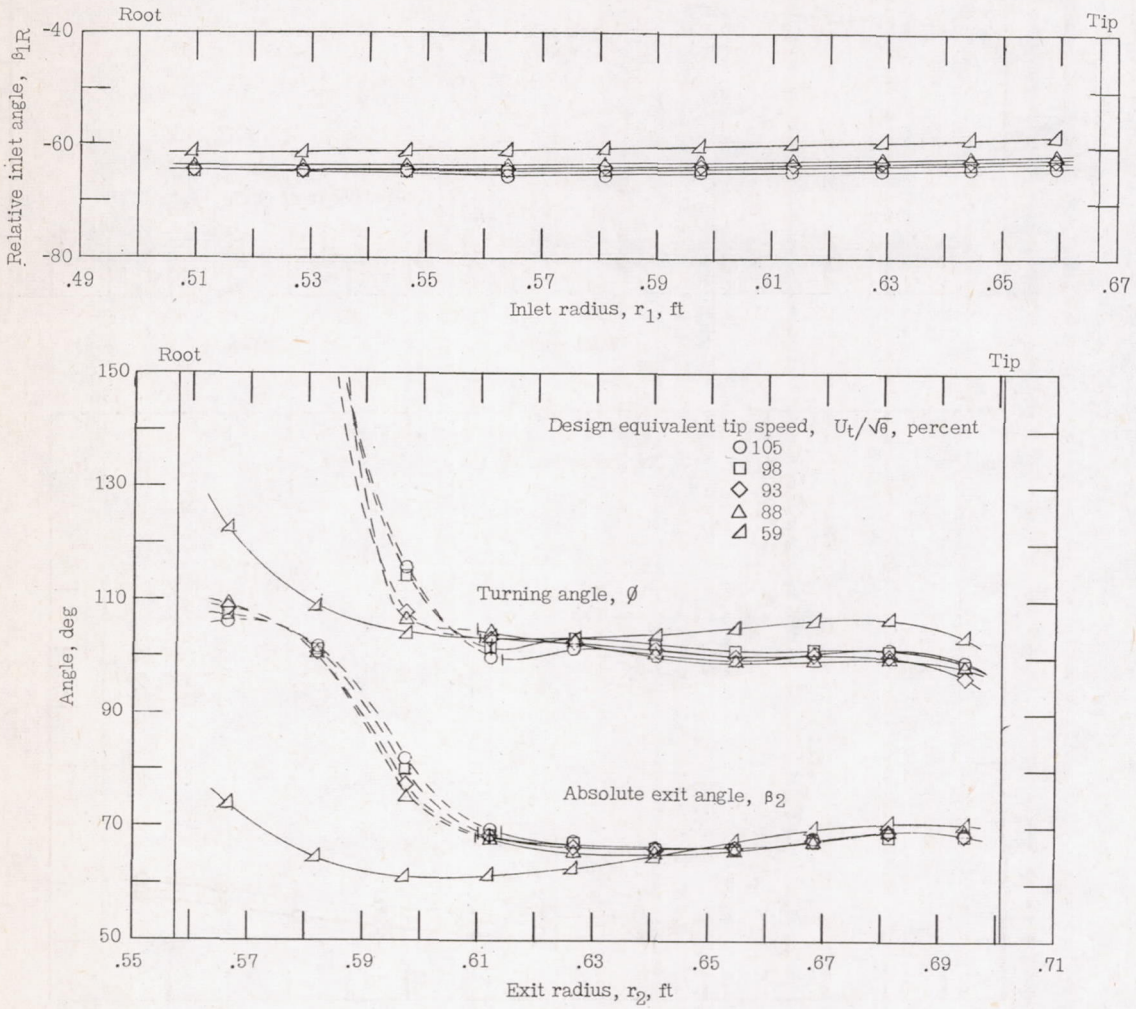
Figure 10.- Effect of back pressure on static pressure distribution along outer casing for rotor operating with guide vanes.





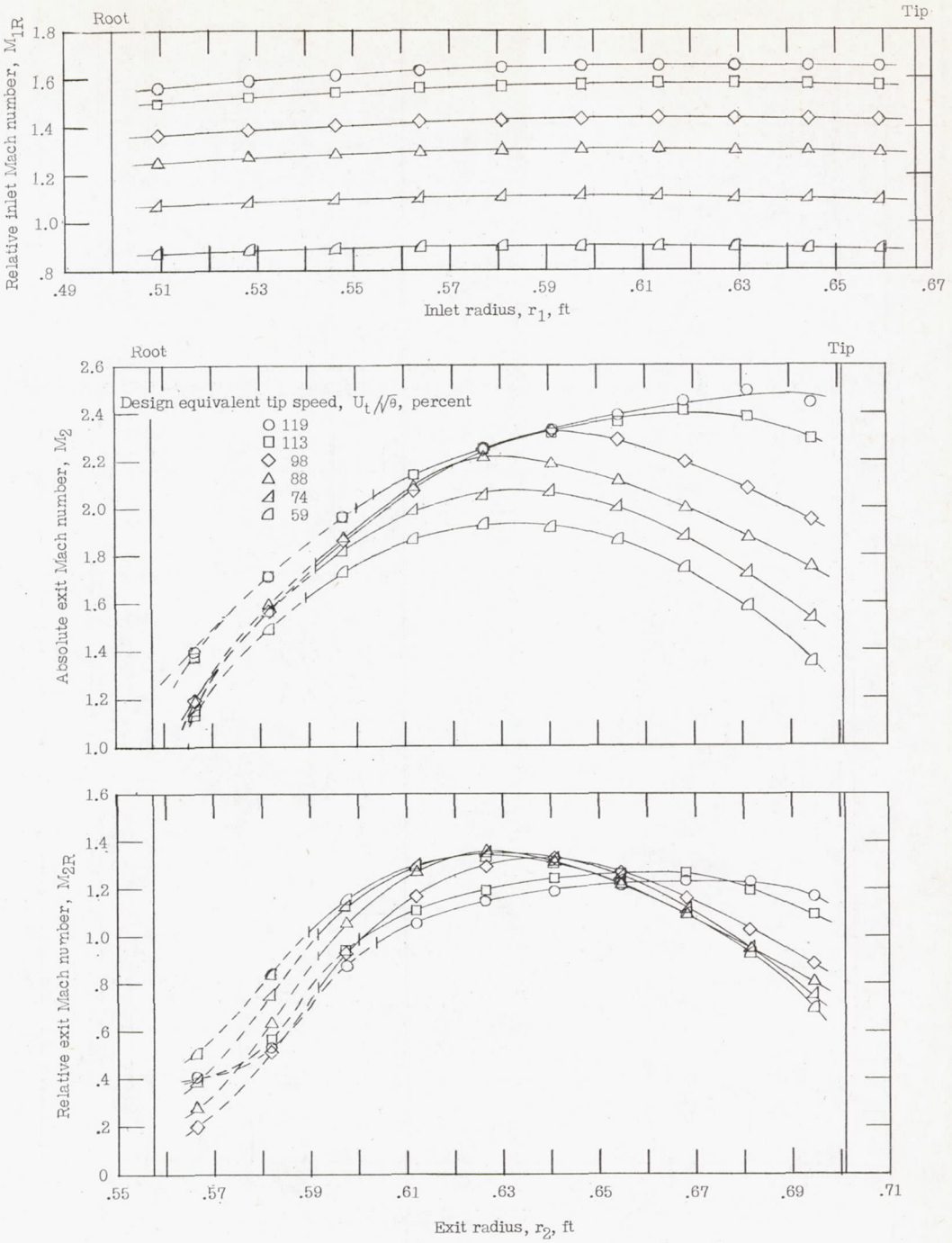
(a) Open throttle.

Figure 11.- Radial variation of flow angles for rotor operating with guide vanes over a range of equivalent tip speeds.



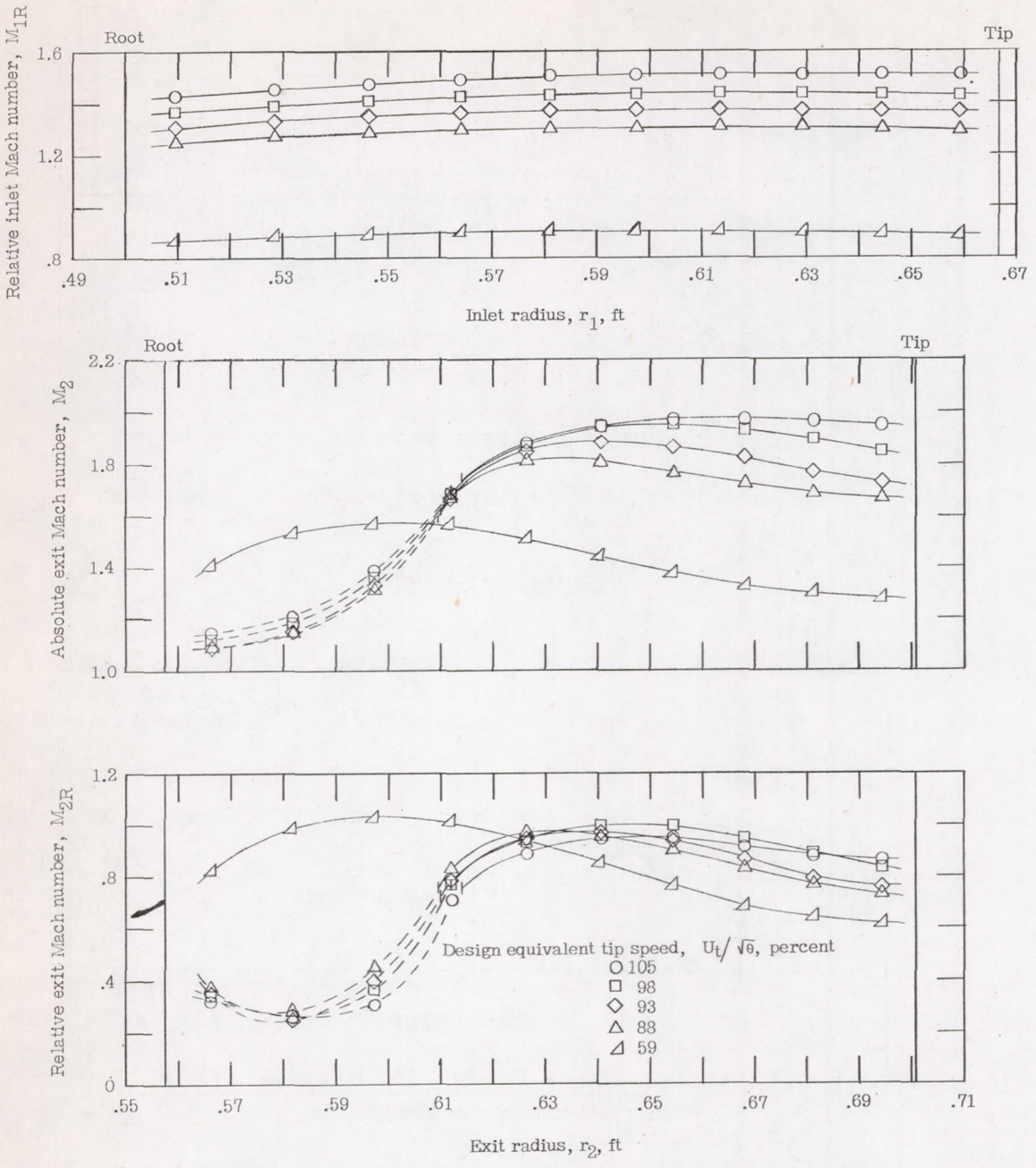
(b) Maximum throttle.

Figure 11.- Concluded.



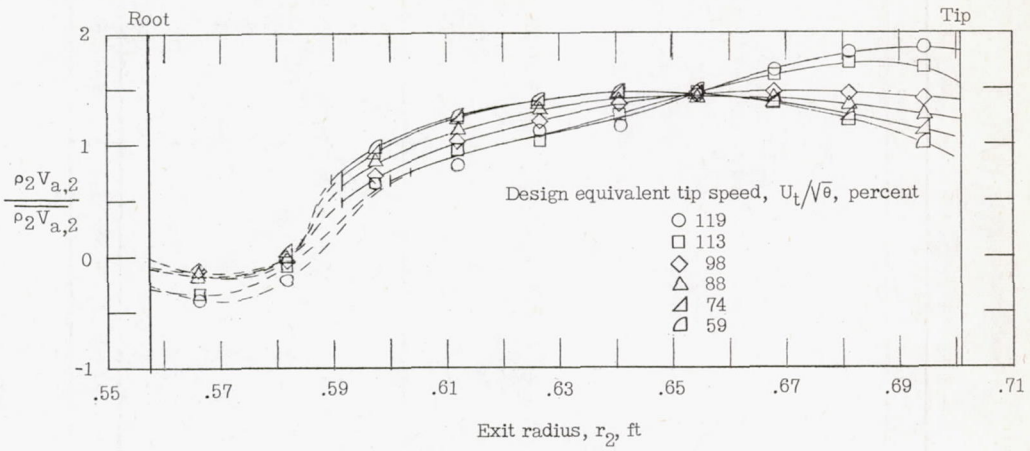
(a) Open throttle.

Figure 12.- Radial variation Mach number for rotor operating with guide vanes over a range of equivalent tip speeds.

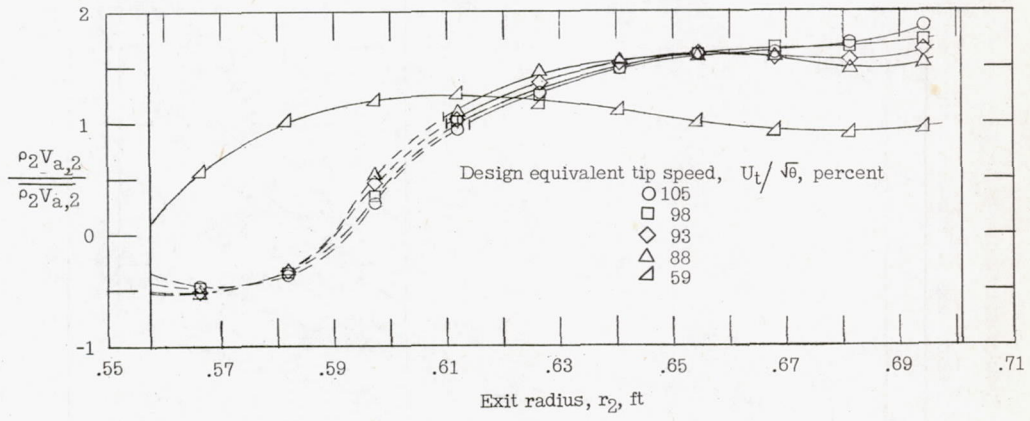


(b) Maximum throttle.

Figure 12.- Concluded.

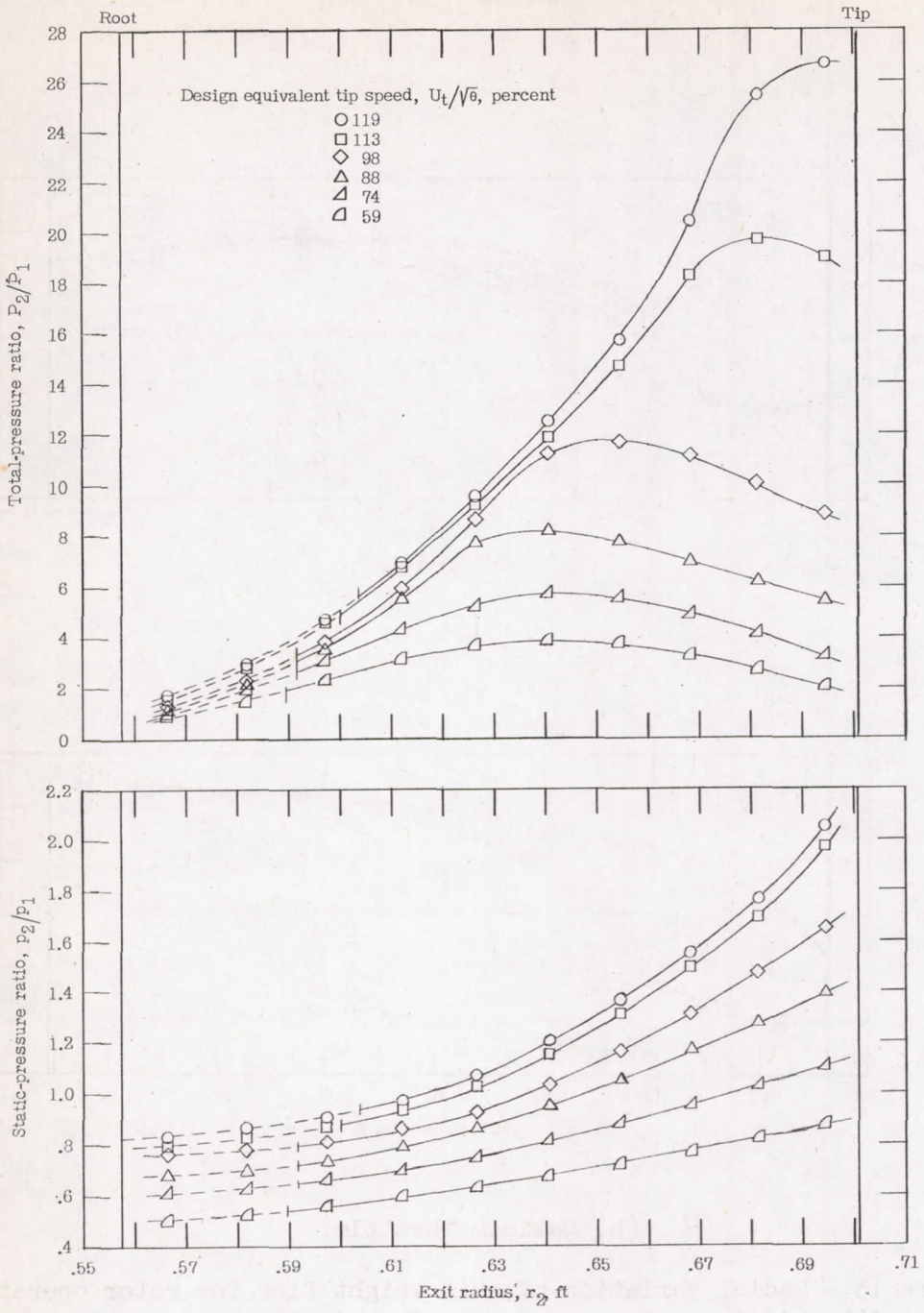


(a) Open throttle.



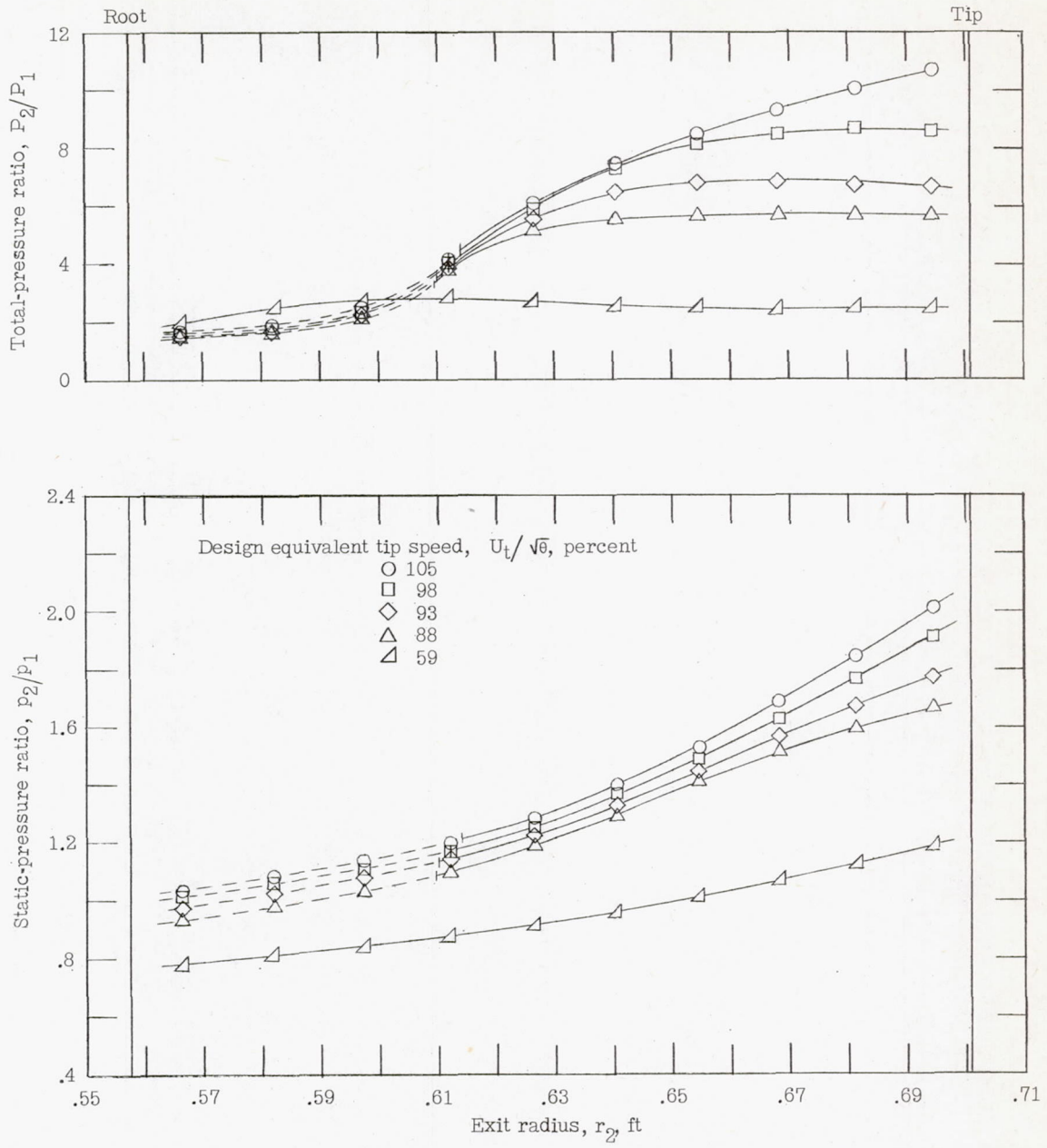
(b) Maximum throttle.

Figure 13.- Radial variation of exit weight flow for rotor operating with guide vanes over a range of equivalent tip speeds.



(a) Open throttle.

Figure 14.- Radial variation of pressure ratio for rotor operating with guide vanes over a range of equivalent tip speeds.



(b) Maximum throttle.

Figure 14.- Concluded.

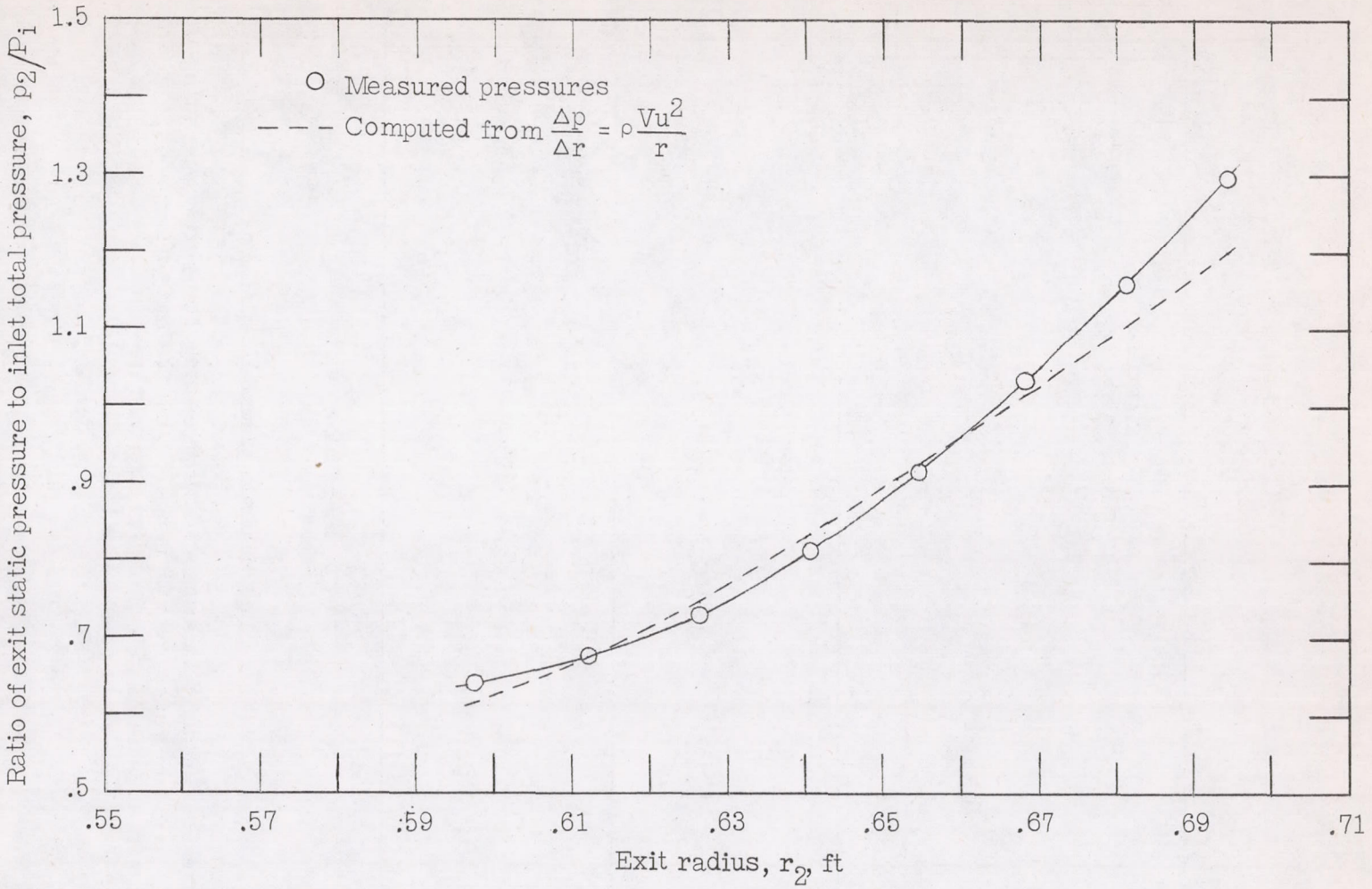
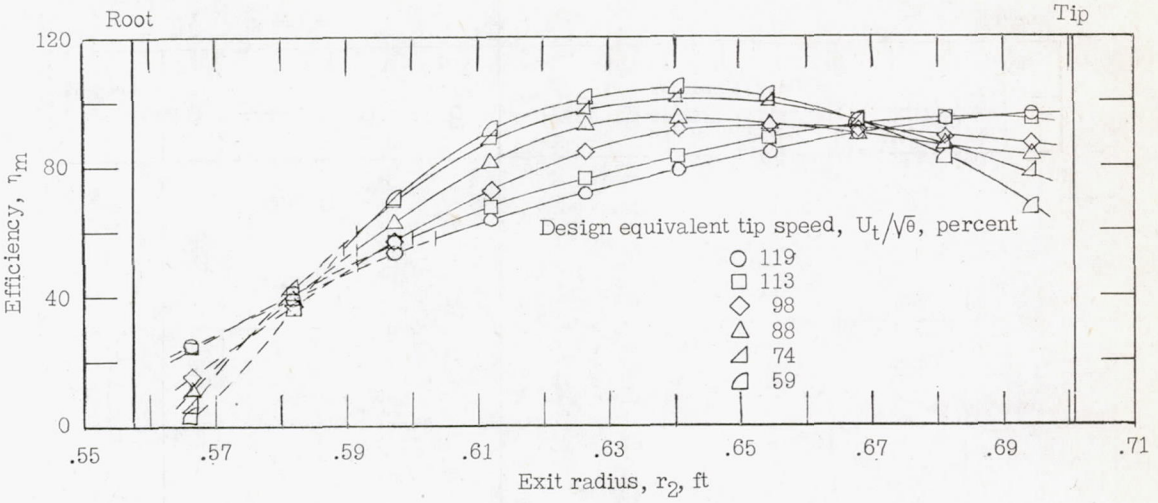
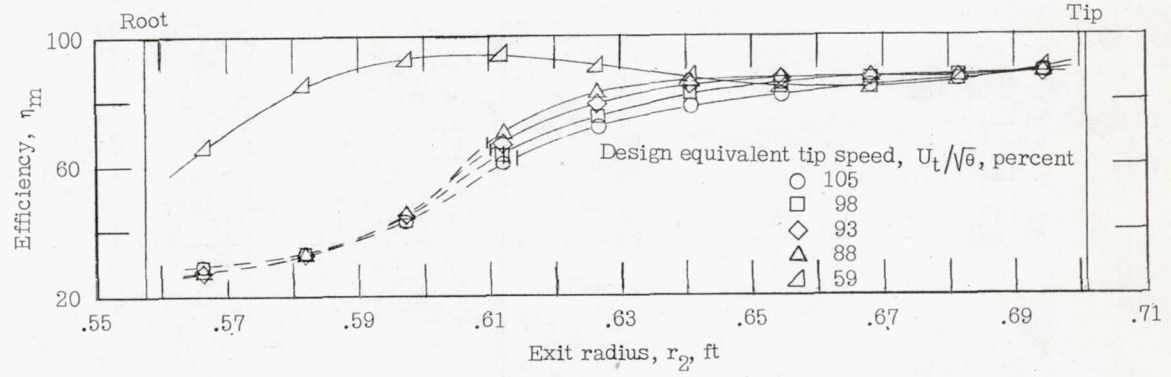


Figure 15.- Radial variation of exit static pressure at 98 percent of design speed for rotor operating with guide vanes.

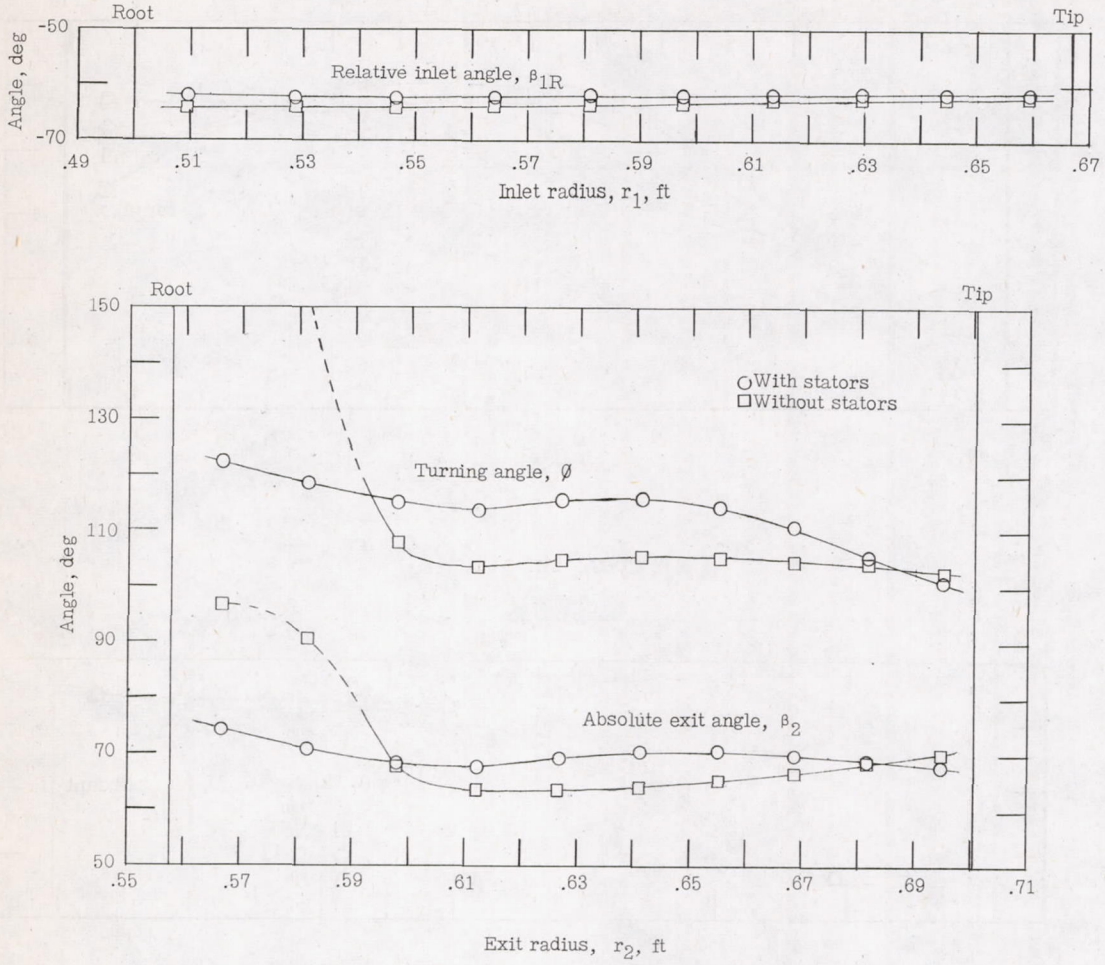


(a) Open throttle.



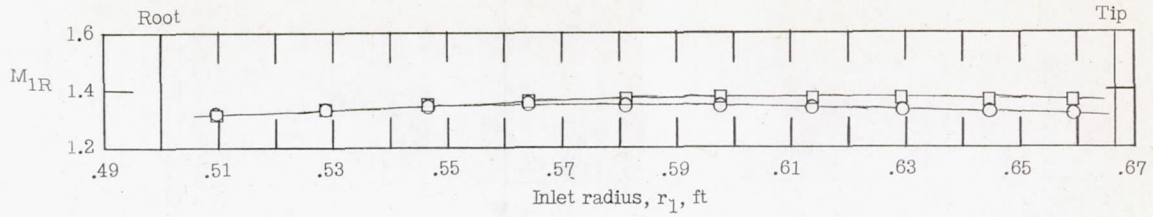
(b) Maximum throttle.

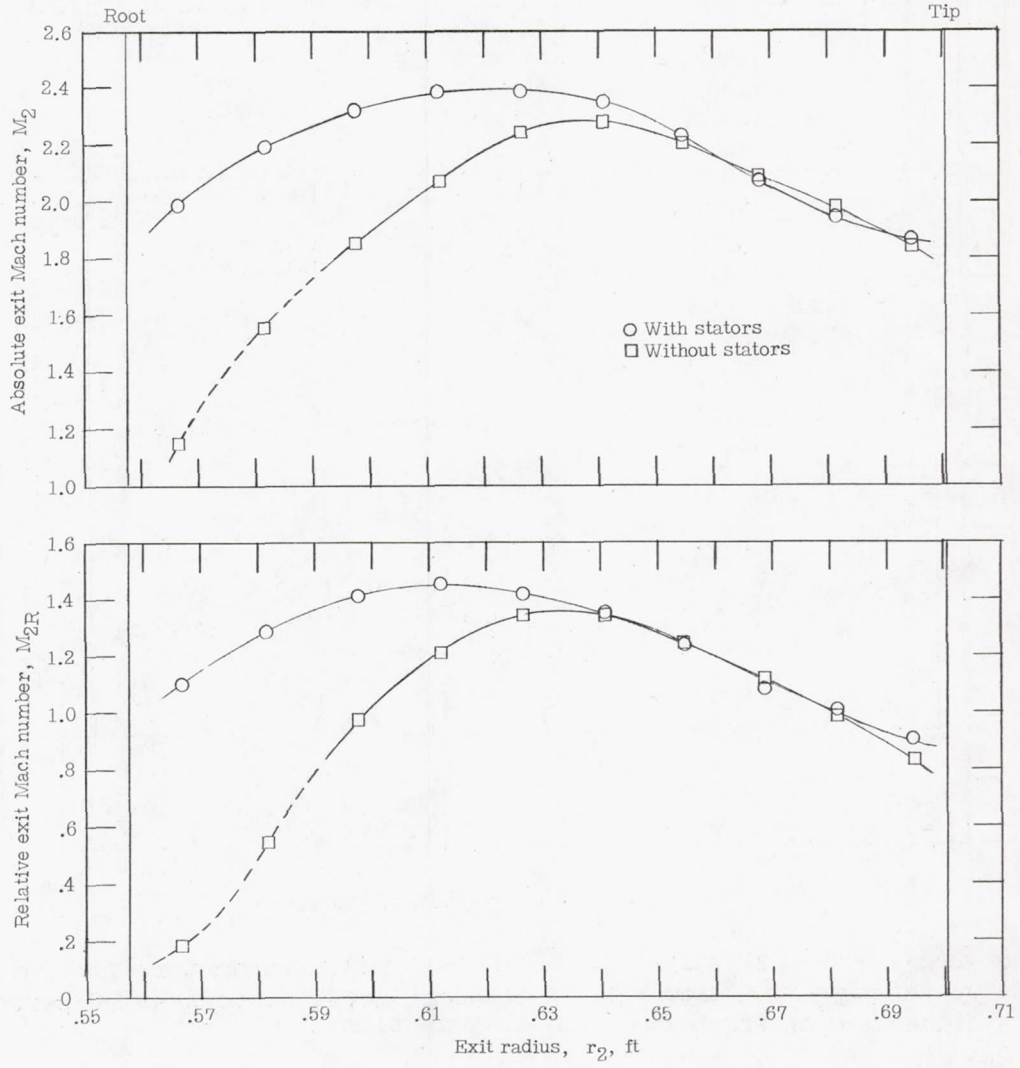
Figure 16.- Radial variation of efficiency for rotor operating with guide vanes over a range of equivalent tip speeds.



(a) Angle distribution.

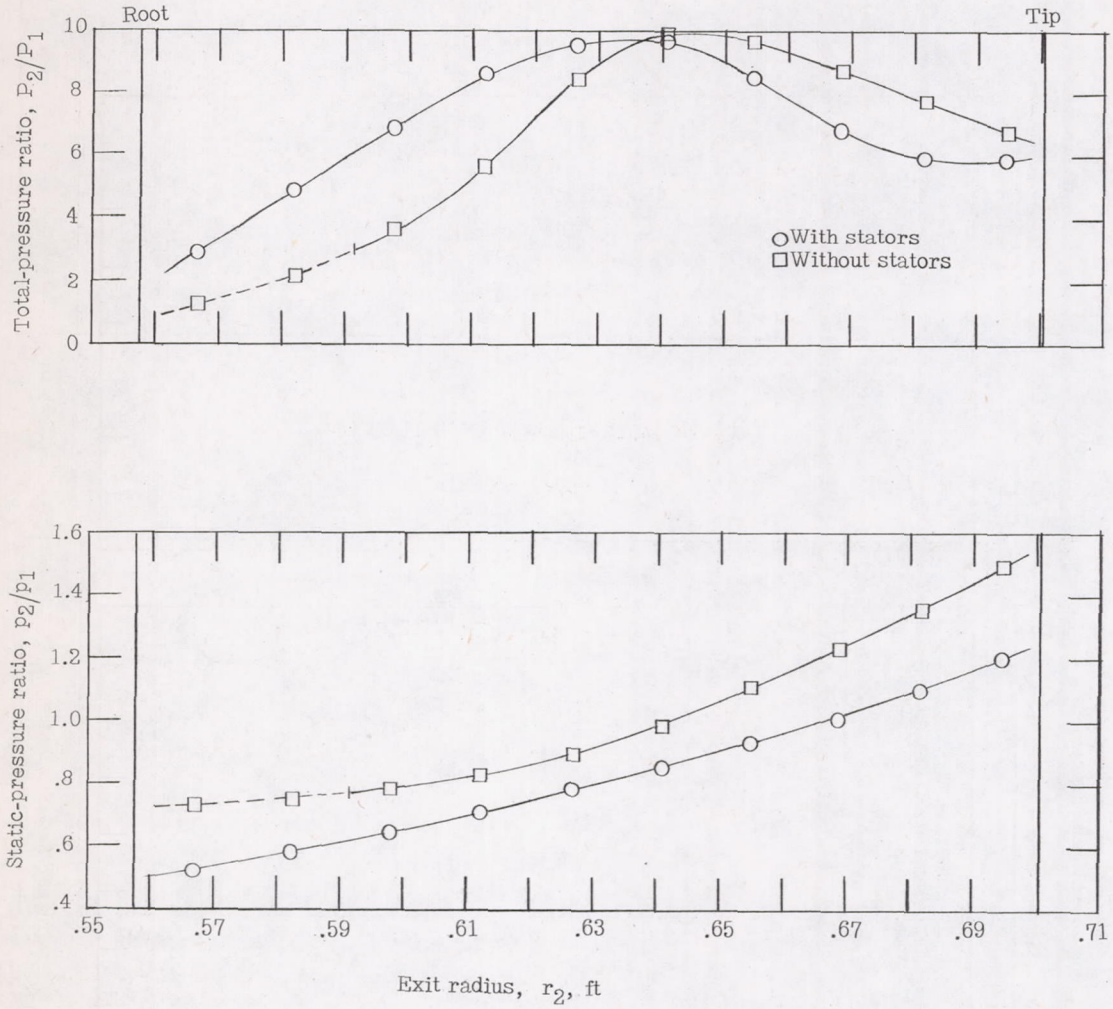
Figure 17.- Radial variation of several rotor parameters for rotor operating with guide vanes and sheet-metal stators at 92 percent of design speed.





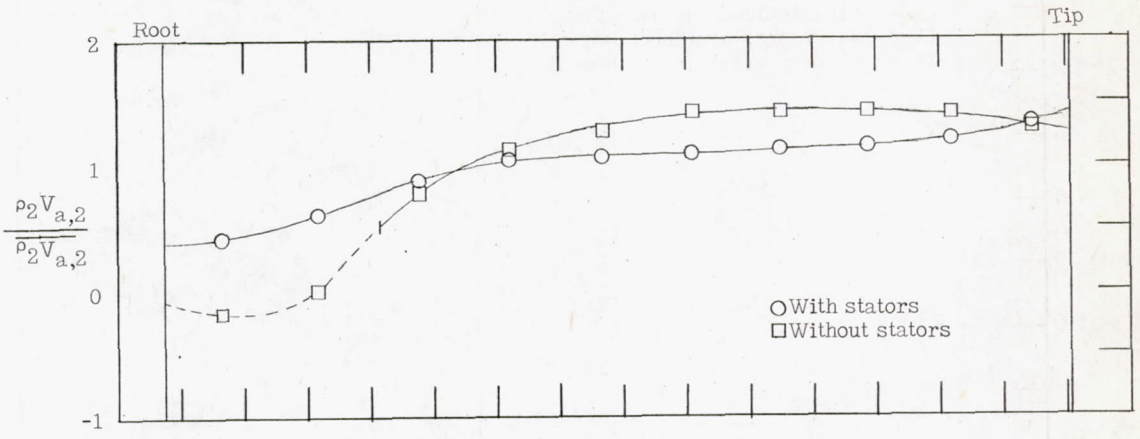
(b) Mach number distribution.

Figure 17.- Continued.

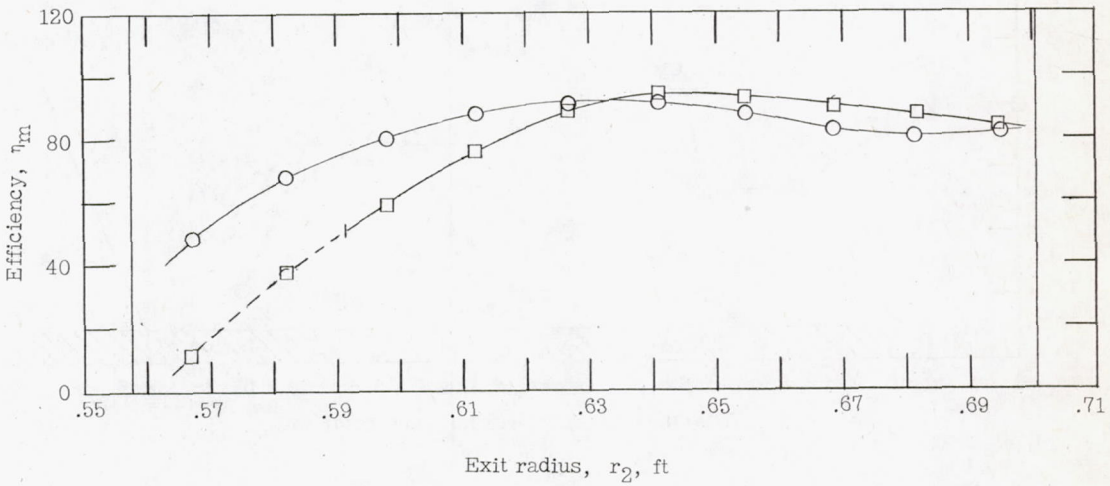


(c) Pressure-ratio distribution.

Figure 17.- Continued.



(d) Weight-flow distribution.



(e) Efficiency distribution.

Figure 17.- Concluded.

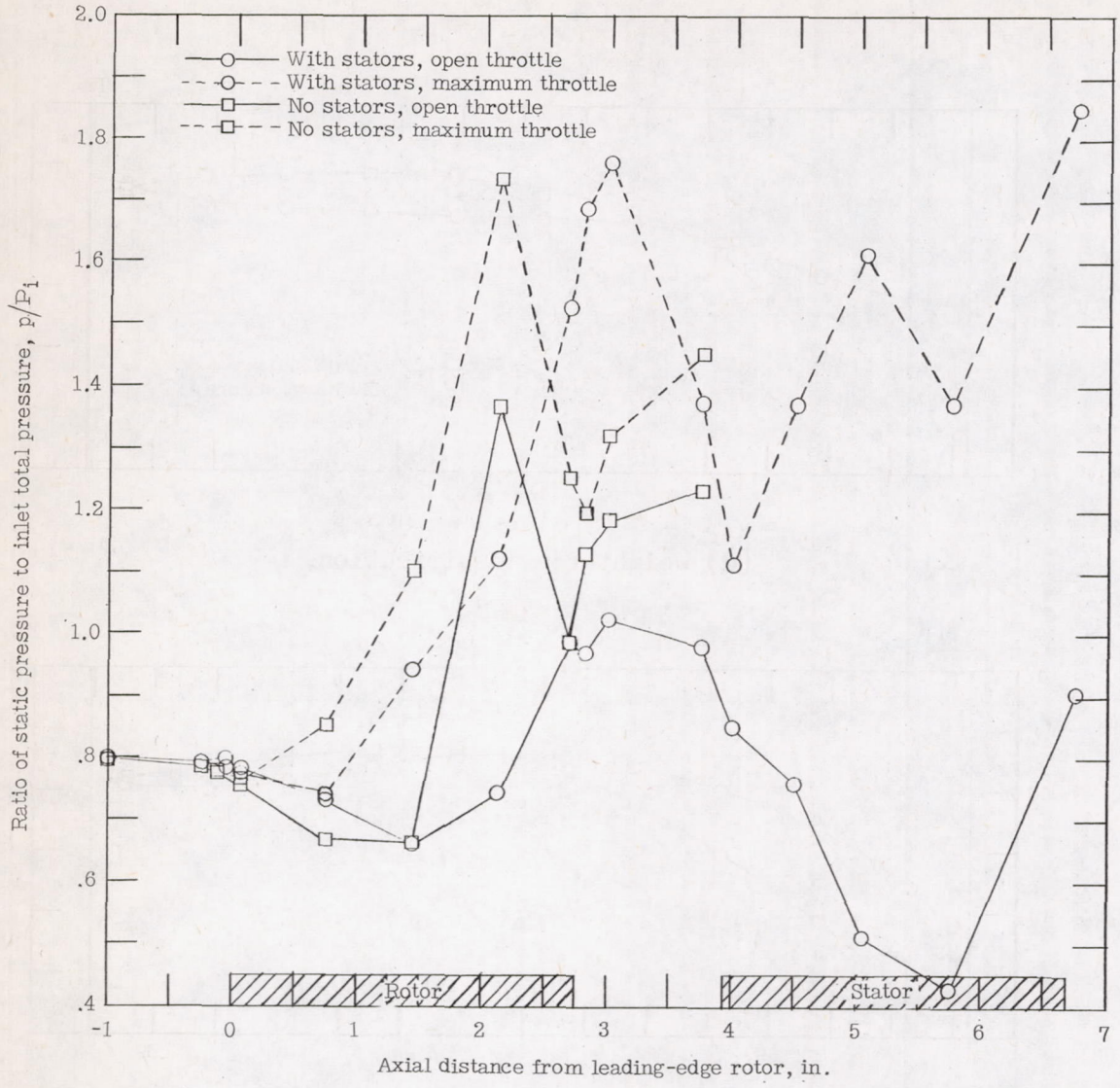


Figure 18.- Static-pressure distribution along outer casing for impulse rotor operating with guide vanes at 91 percent of design speed.

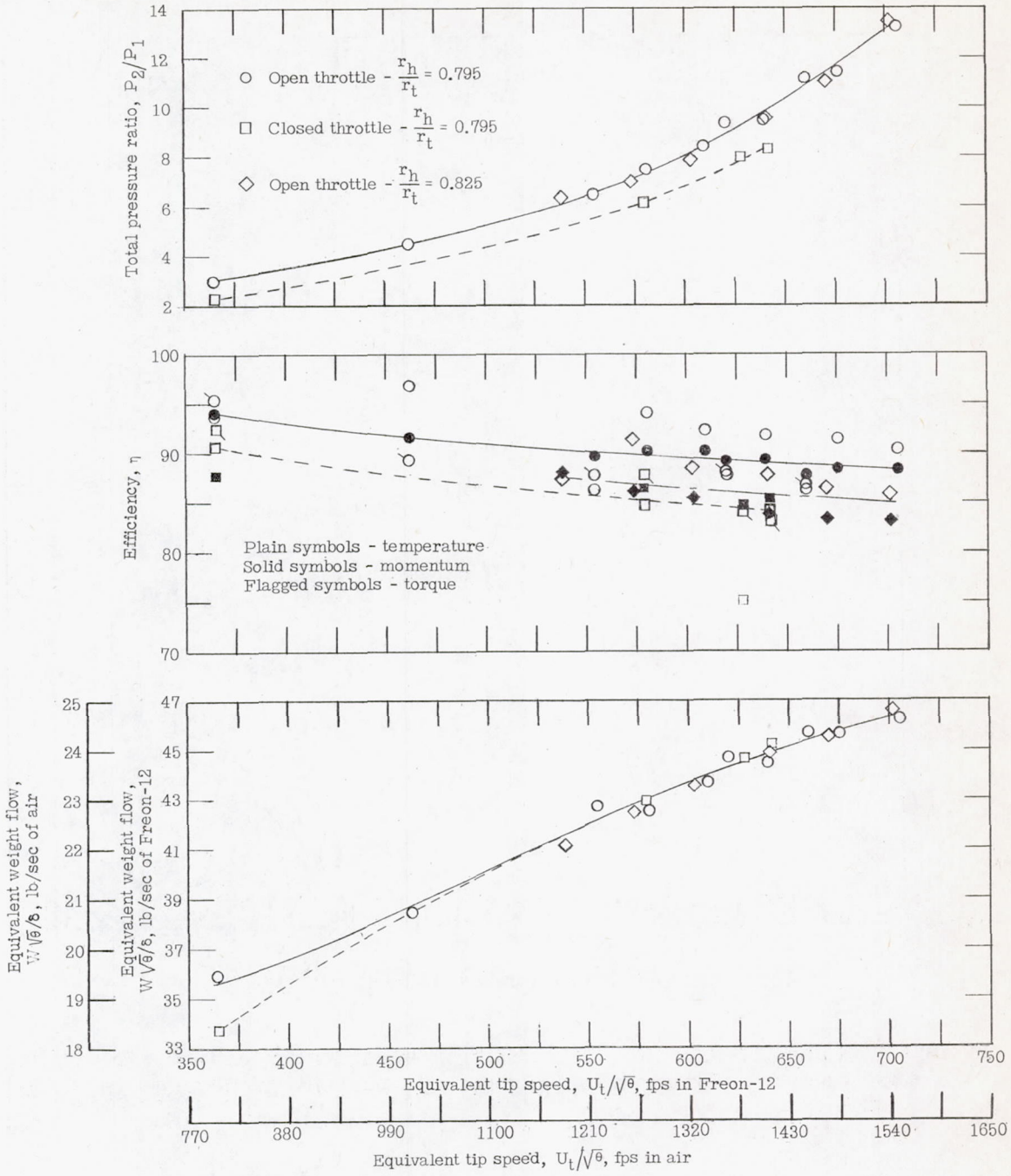
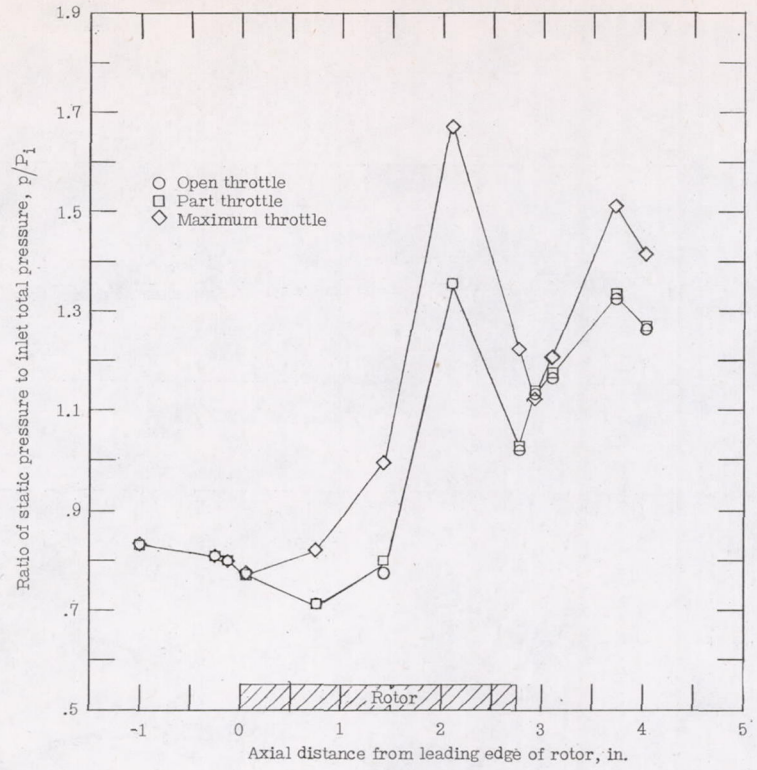
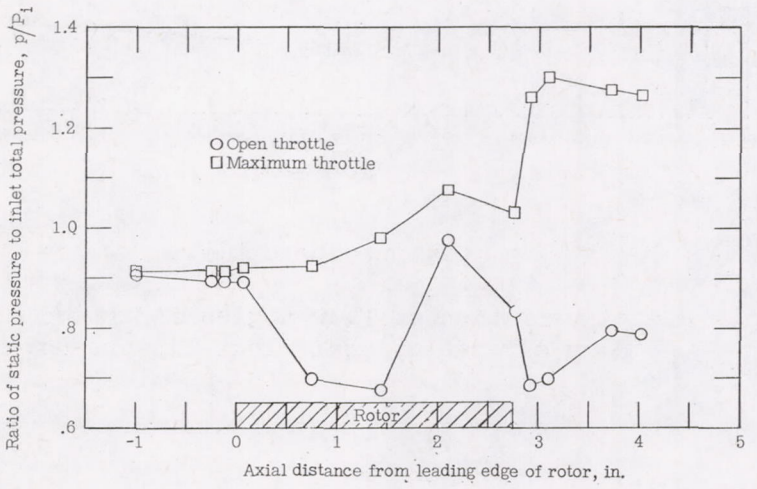


Figure 19.- Characteristics of rotor alone for original and modified hub contours.

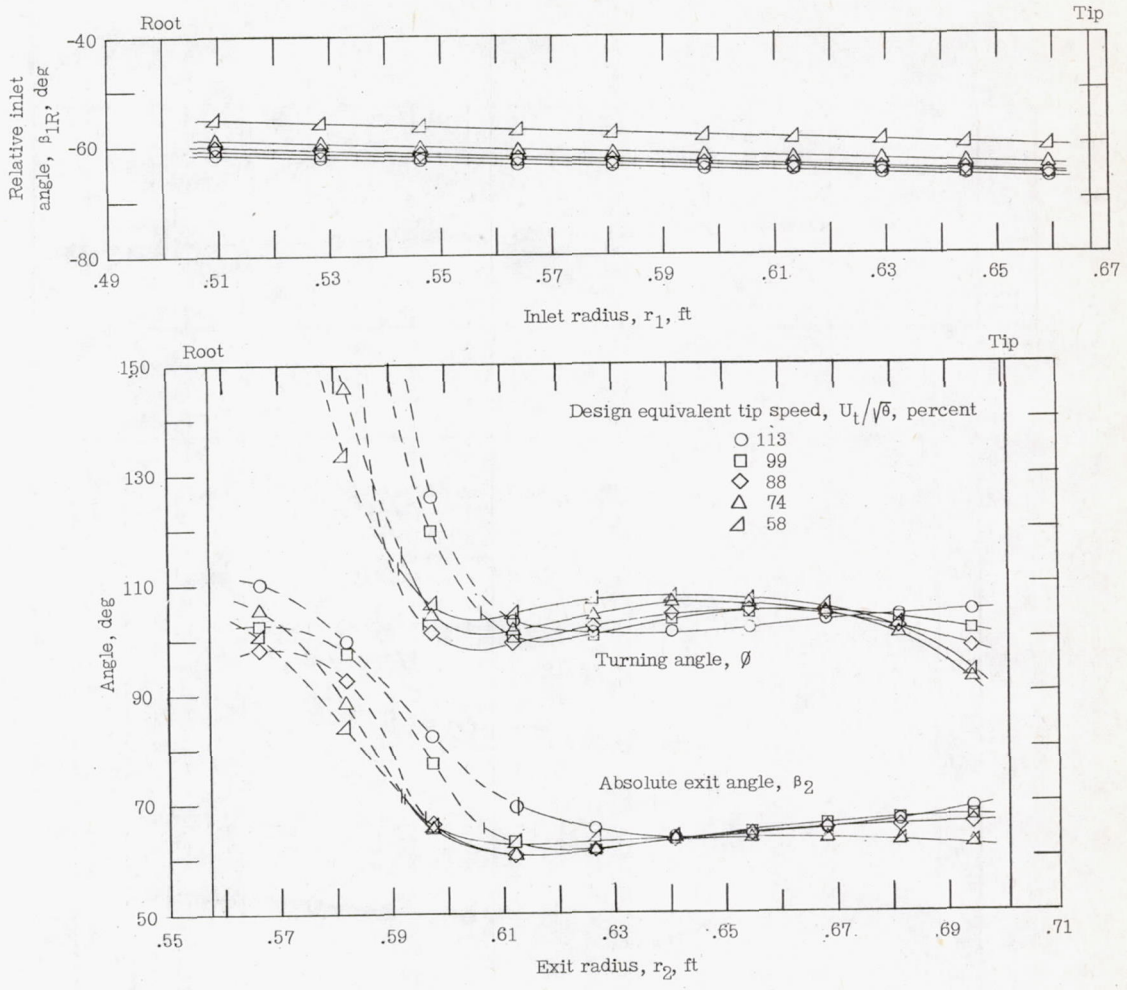


(a) 99 percent of design speed.



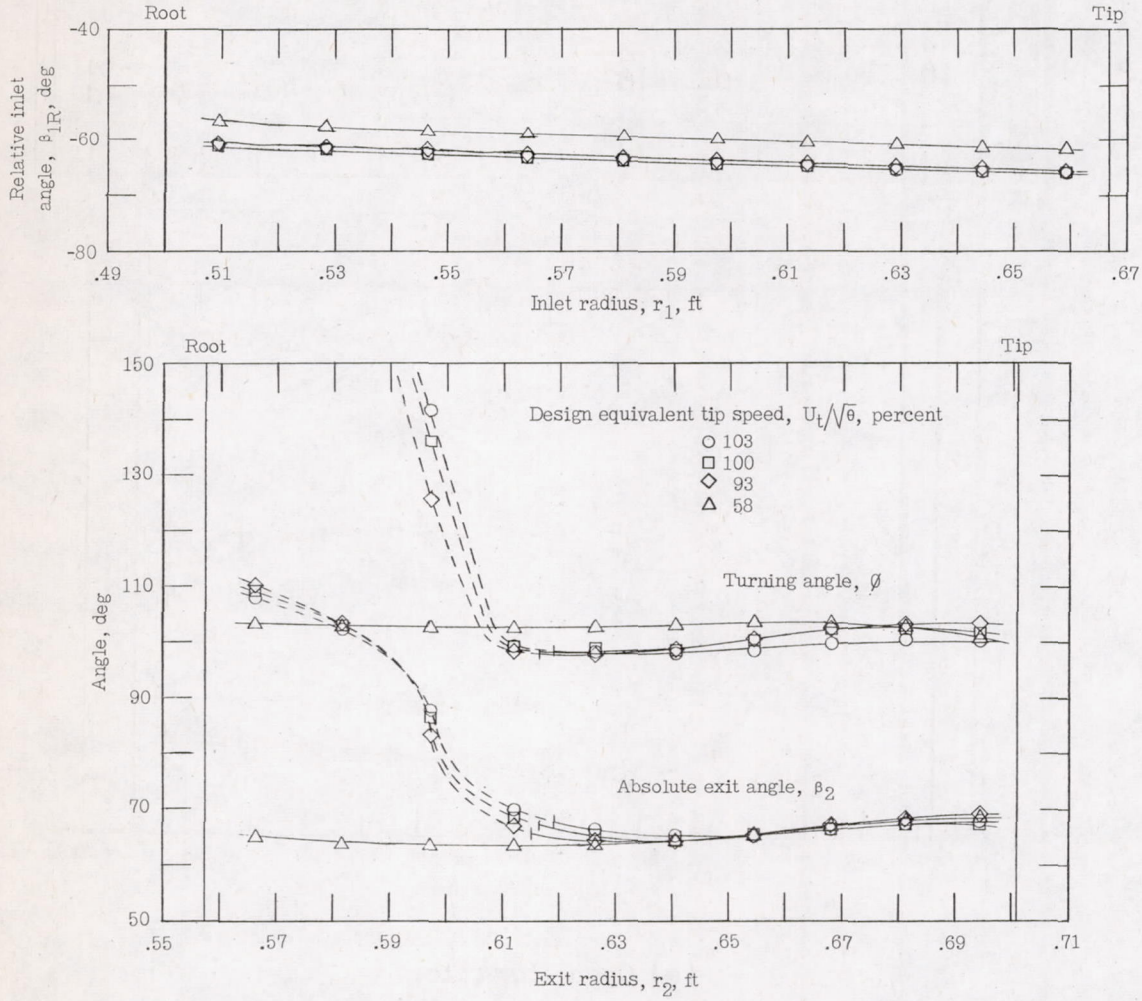
(b) 58 percent of design speed.

Figure 20.- Effect of back pressure on static pressure distribution along outer casing for rotor alone.



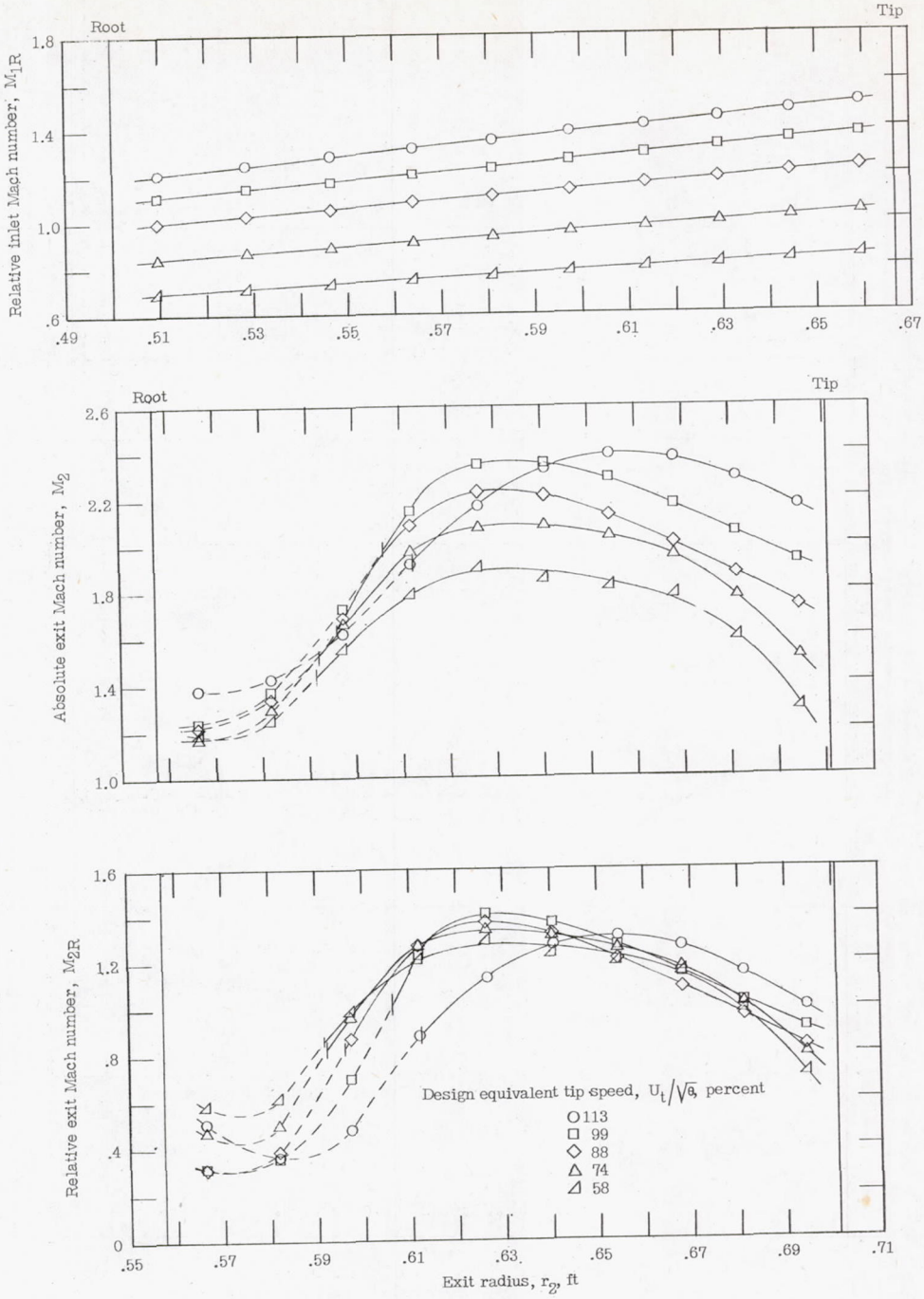
(a) Open throttle.

Figure 21.- Radial variation of flow angles for rotor alone operating over a range of equivalent tip speeds.



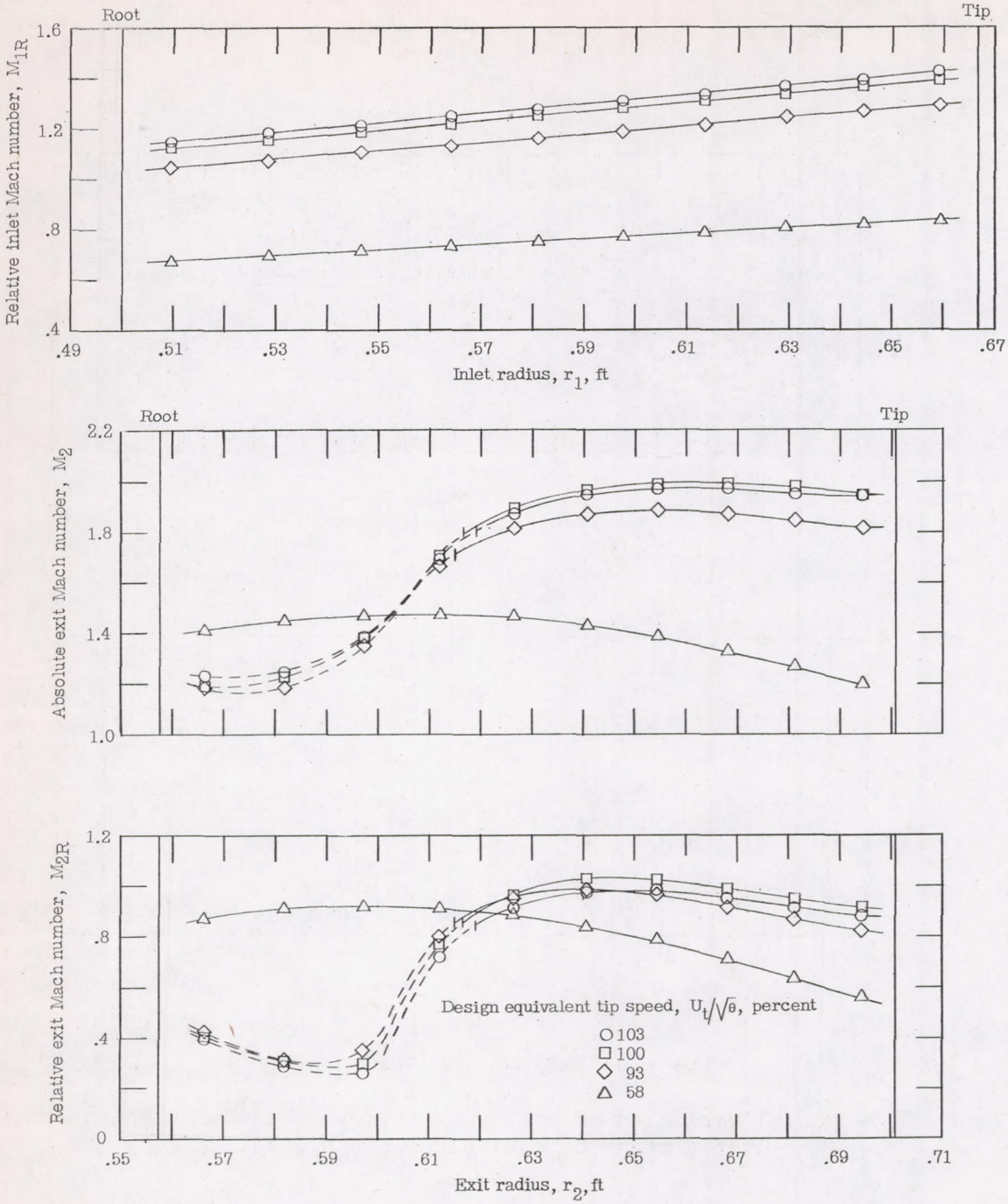
(b) Maximum throttle.

Figure 21.- Concluded.



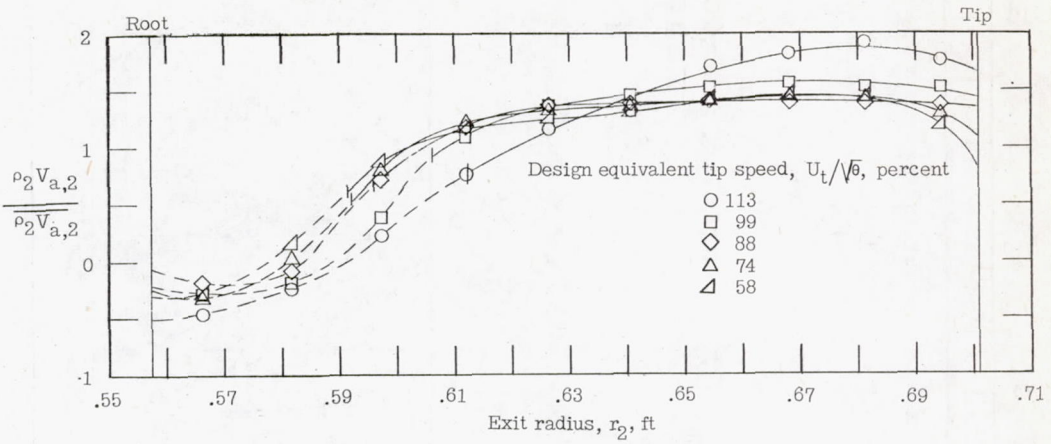
(a) Open throttle.

Figure 22.- Radial variation of Mach number for rotor alone operating over a range of equivalent tip speeds.

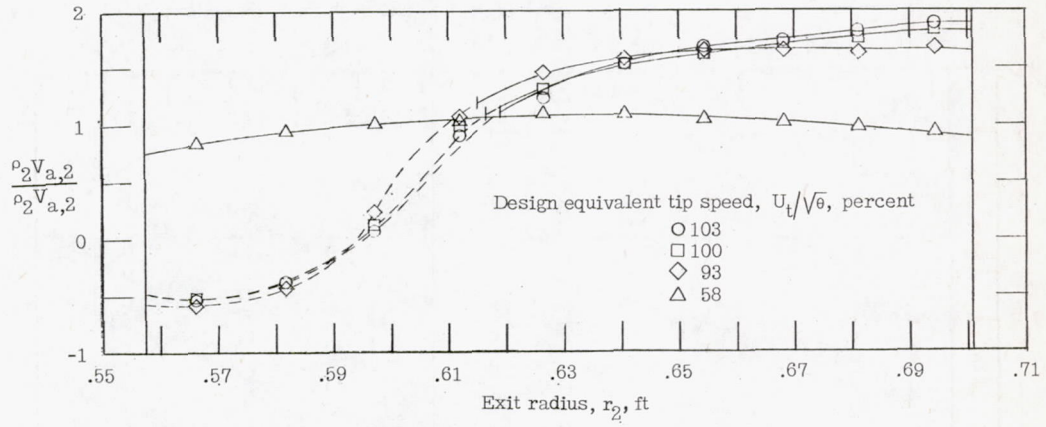


(b) Maximum throttle.

Figure 22.- Concluded.

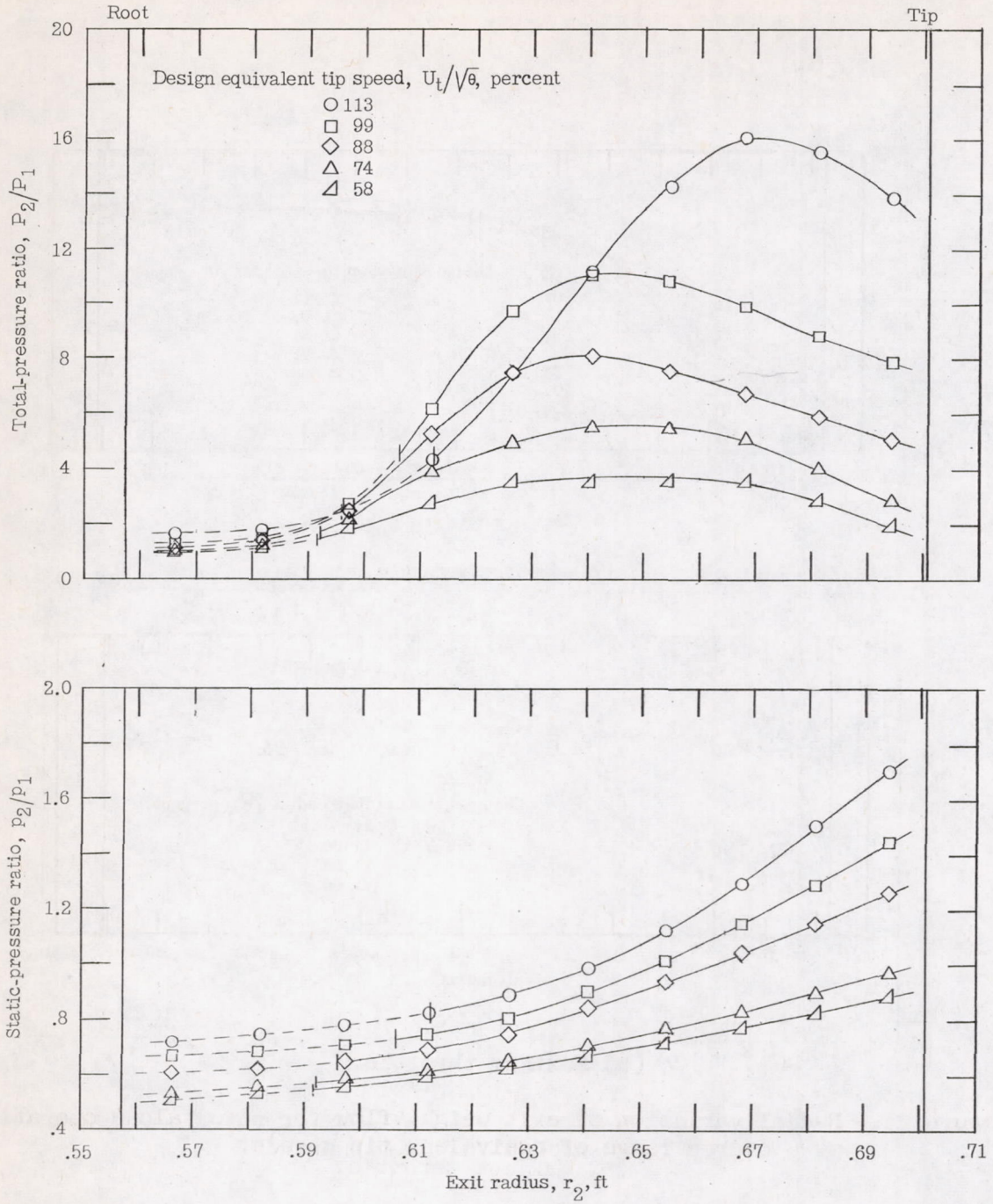


(a) Open throttle.



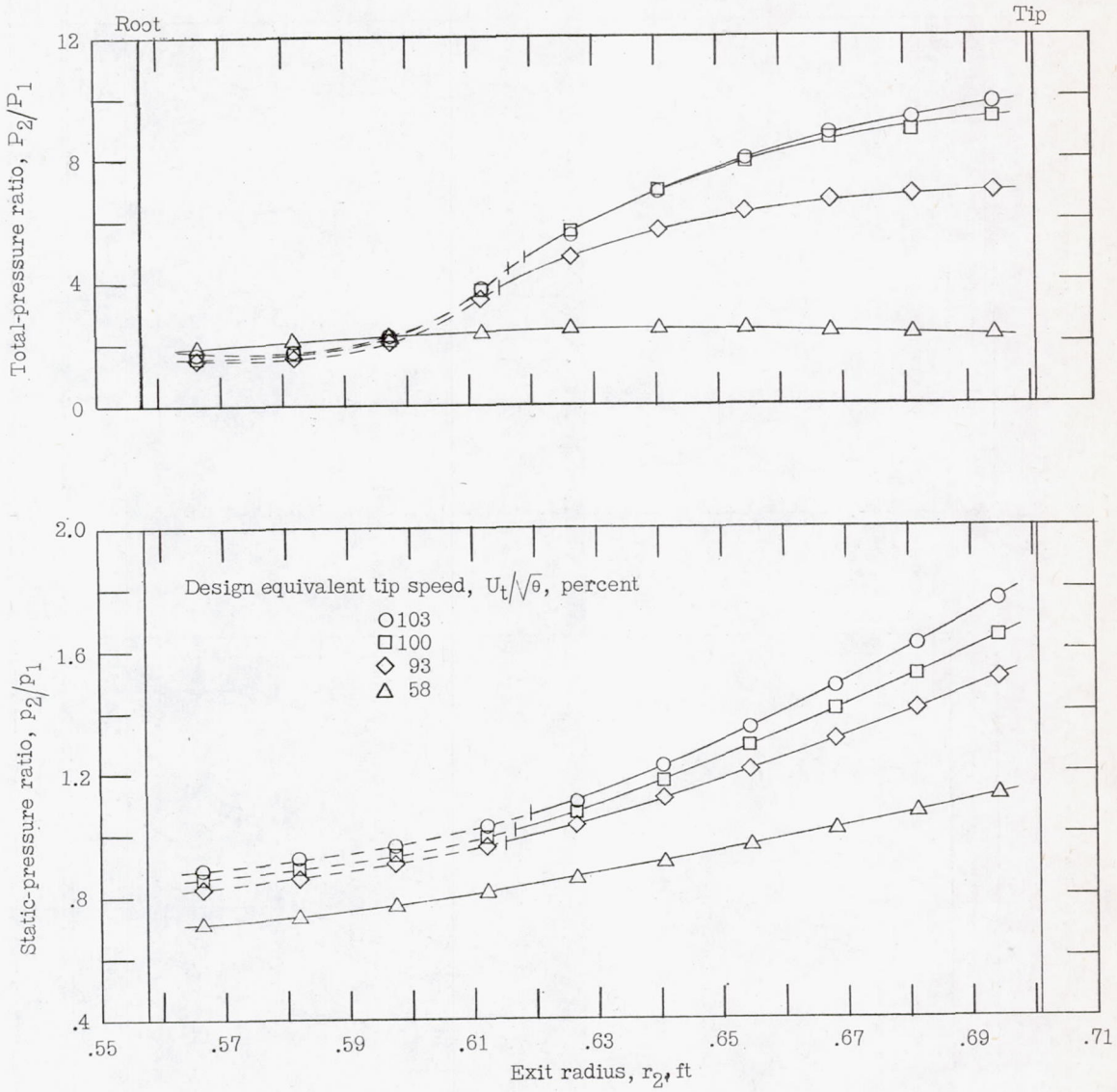
(b) Maximum throttle.

Figure 23.- Radial variation of exit weight flow for rotor alone operating over a range of equivalent tip speeds.



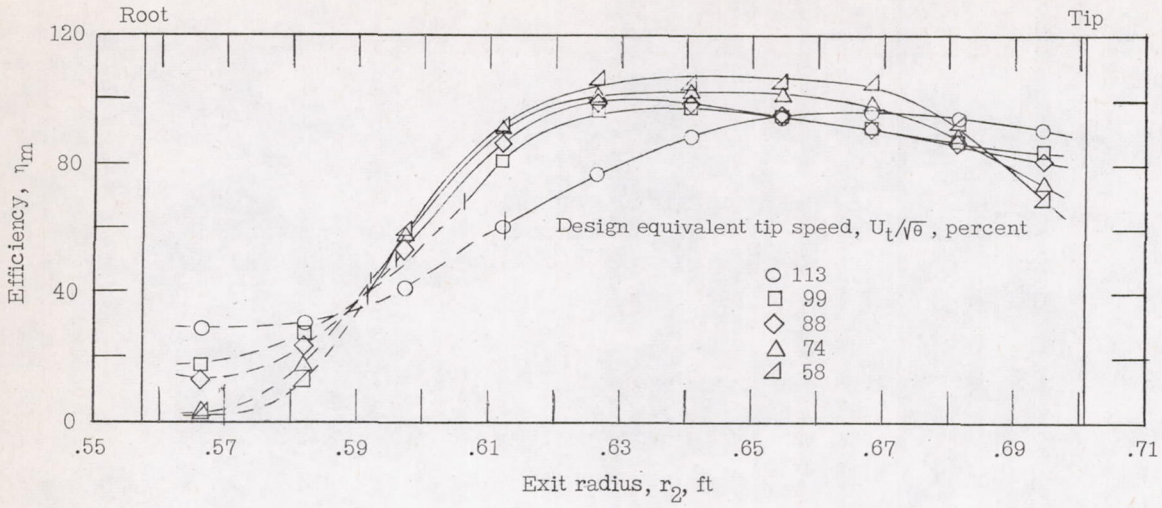
(a) Open throttle.

Figure 24.- Radial variation of pressure ratio for rotor alone operating over a rangle of equivalent tip speeds.

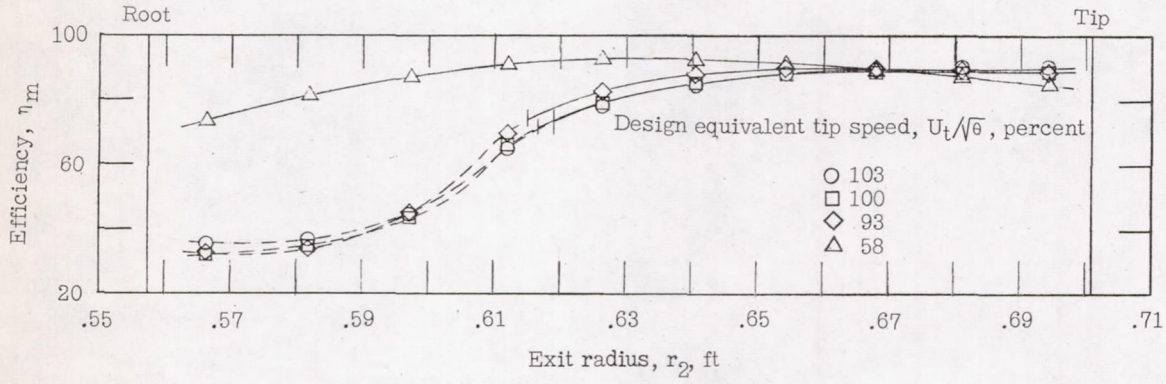


(b) Maximum throttle.

Figure 24.- Concluded.



(a) Open throttle.



(b) Maximum throttle.

Figure 25.- Radial variation of efficiency for rotor alone operating over a range of equivalent tip speeds.

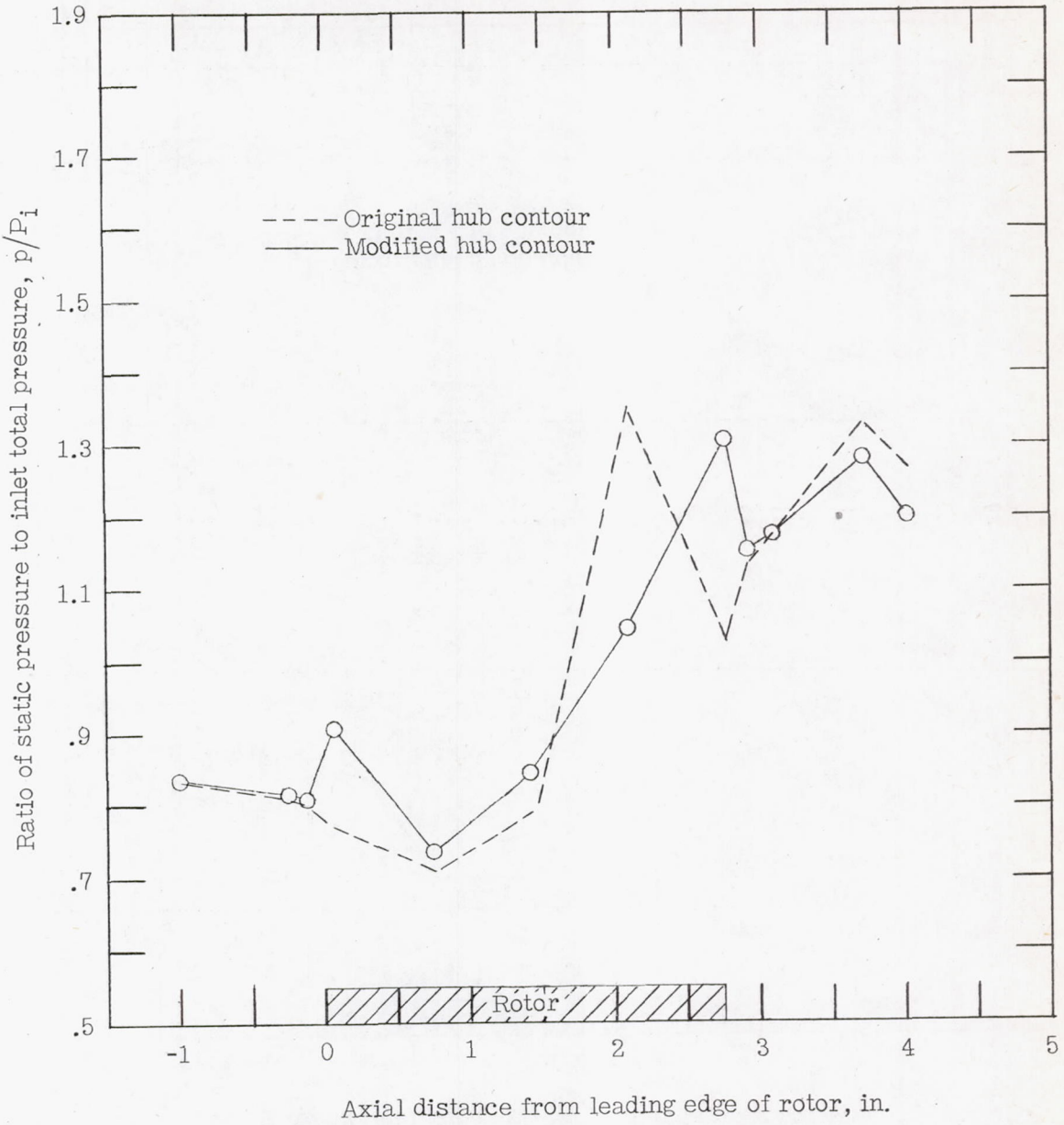


Figure 26.- Comparison of static pressure distributions along outer casing for rotor with original and modified hub contours operating at open throttle at 99 percent of design speed.

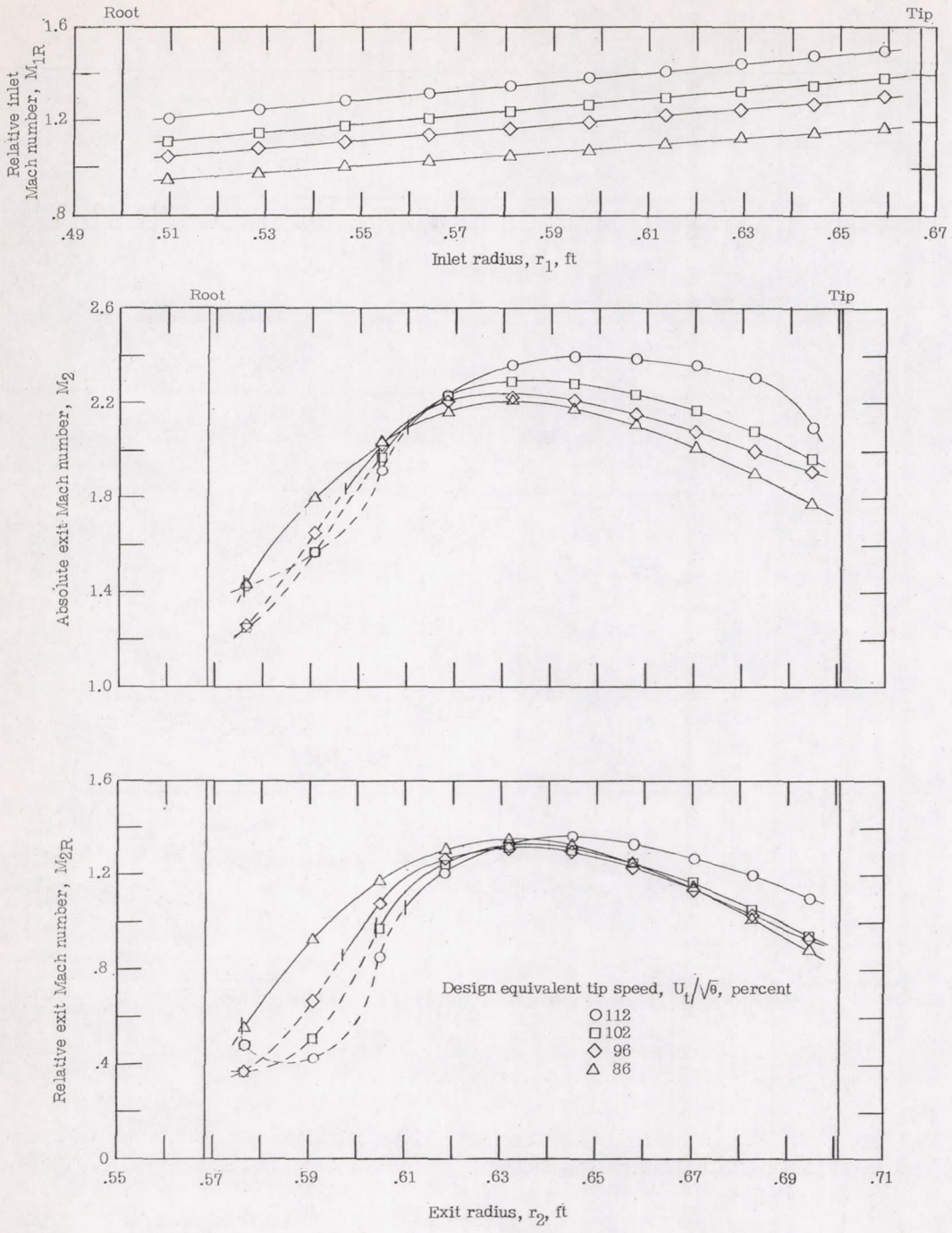


Figure 27.- Radial distribution of Mach number for rotor alone with modified hub contour operating at open throttle over a range of equivalent tip speeds.

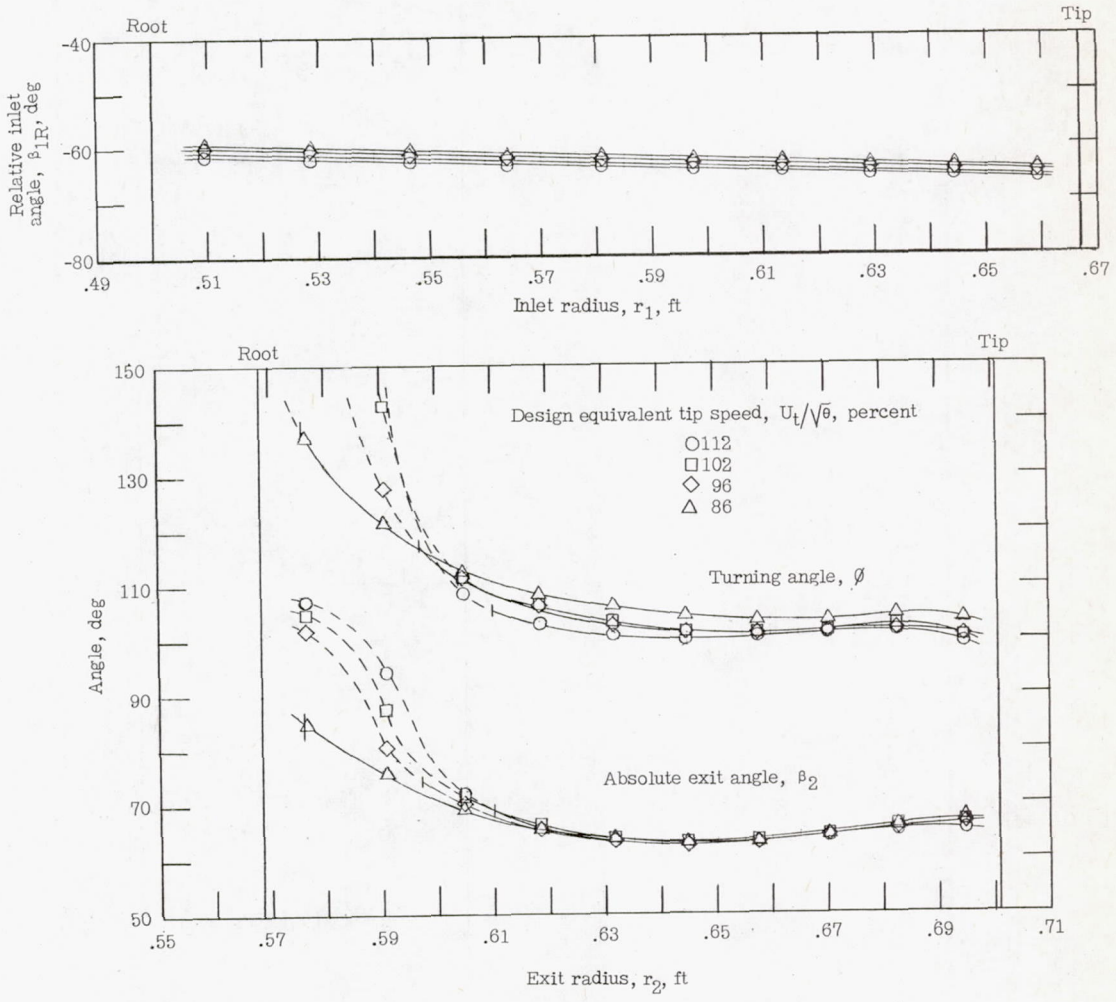


Figure 28.- Radial distribution of flow angles for rotor alone with modified hub contour operating at open throttle over a range of equivalent tip speeds.

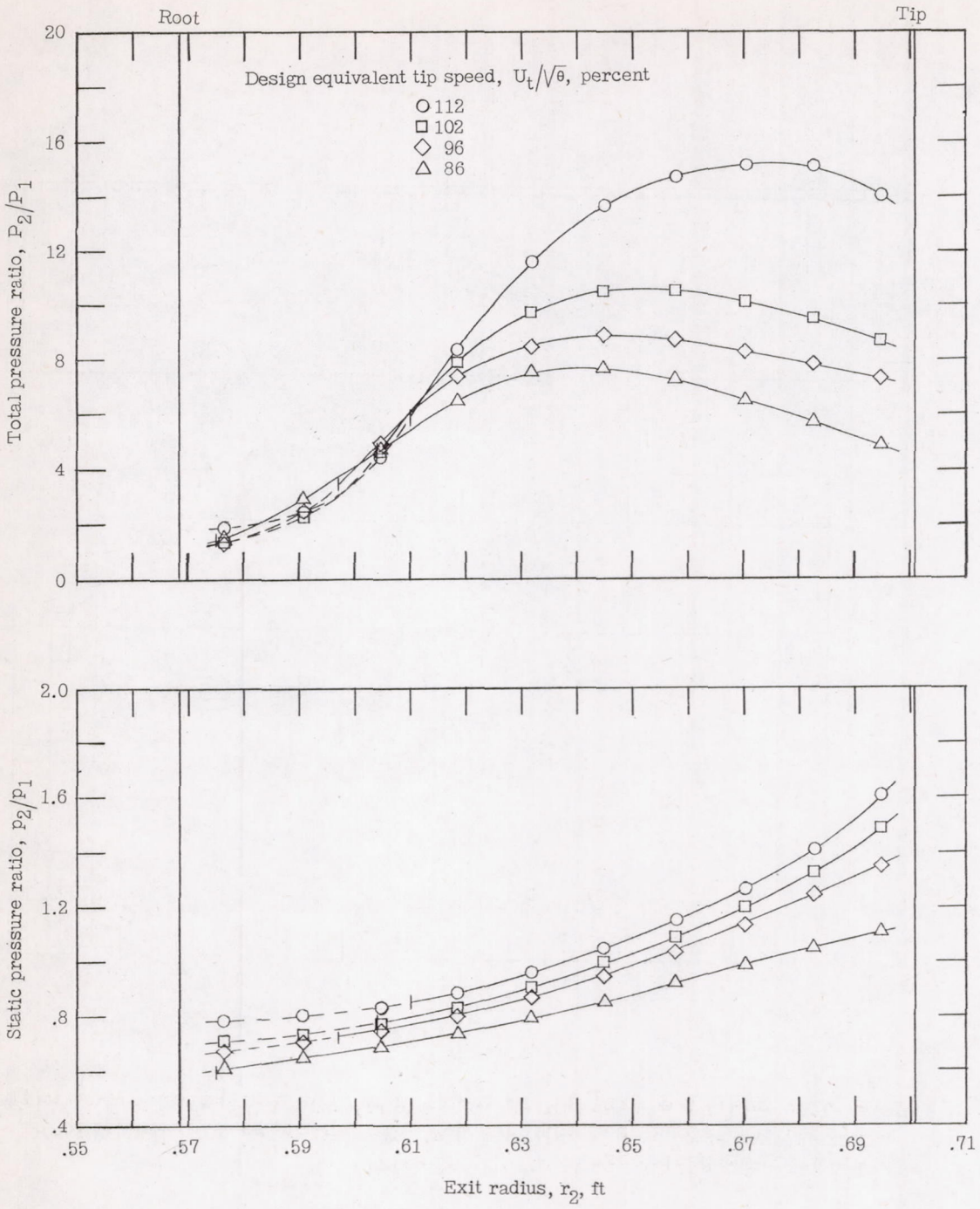


Figure 29.- Radial variation of pressure ratio for rotor alone with modified hub contour operating at open throttle over a range of equivalent tip speeds.

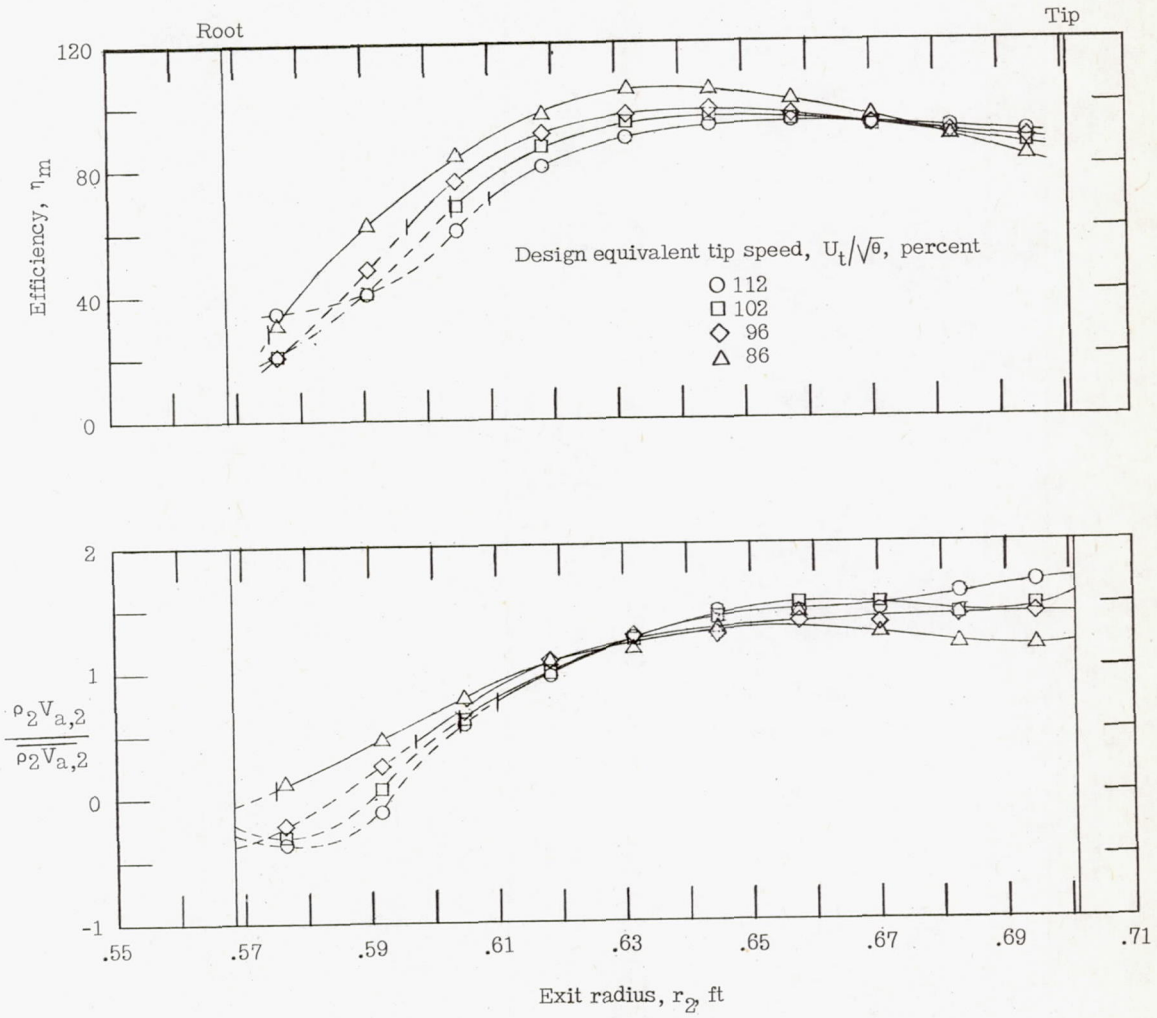


Figure 30.- Radial variation of efficiency and exit weight flow for rotor alone with modified hub contour operating at open throttle over a range of equivalent tip speeds.